Numerical analysis of ion temperature effects to the plasma wall transition using a one-dimensional two-fluid model. I. Finite Debye to ionization length ratio

T. Gyergyek[1,2] and J. Kovačič[2]
[1]*Faculty of Electrical Engineering, University of Ljubljana, Tržaška 25, 1000 Ljubljana, Slovenia*
[2]*Jožef Stefan Institute, Jamova 39, P.O. Box 100, 1000 Ljubljana, Slovenia*

(Received 24 February 2017; accepted 9 May 2017; published online 6 June 2017)

A one-dimensional, two-fluid, steady state model is used for the analysis of ion temperature effects to the plasma-wall transition. In this paper, the model is solved for a finite ratio ε between the Debye and the ionization length, while in Part II [T. Gyergyek and J. Kovačič, Phys Plasmas 24, 063506 (2017)], the solutions for $\varepsilon = 0$ are presented. Ion temperature is treated as a given, independent parameter and it is included in the model as a boundary condition. It is shown that when the ion temperature larger than zero is selected, the ion flow velocity and the electric field at the boundary must be consistent with the selected ion temperature. A numerical procedure, how to determine such "consistent boundary conditions," is proposed, and a simple relation between the ion temperature and ion velocity at the boundary of the system is found. The effects of the ion temperature to the pre-sheath length, potential, ion temperature, and ion density drops in the pre-sheath and in the sheath are investigated. It is concluded that larger ion temperature results in a better shielding of the plasma from the wall. An attempt is made to include the ion heat flux q_i into the model in its simplest form $q_i = -K' \frac{dT_i}{dx}$, where K' is a constant heat conduction coefficient. It is shown that inclusion of such a term into the energy transfer equation introduces an additional ion heating mechanism into the system and the ion flow then becomes isothermal instead of adiabatic even in the sheath. *Published by AIP Publishing*. [http://dx.doi.org/10.1063/1.4984786]

I. INTRODUCTION

The subject of interactions between the plasma and a solid wall and the formation of a boundary layer around it is almost as old as plasma physics itself. In a simple model, confined plasma is brought into contact with an infinitely large, planar, conducting wall. Since the mobility of the electrons is much higher than that of the ions, the wall is bombarded by the background electrons and attains a negative potential with respect to the bulk of the plasma. The negative potential of the wall attracts the ions toward the wall and repels the electrons toward the plasma. In the steady state, a positive space charge forms near the wall to balance the flow of the ions and electrons into the wall.

The plasma-wall transition region can be divided into two separate regions: a neutral pre-sheath adjacent to the plasma and a space charge dominated layer, called sheath, adjacent to the wall.[1,2] The sheath width is usually a few Debye lengths λ_D and its task is to shield the plasma from the wall. The pre-sheath width, on the other hand, is determined by some characteristic mean free path L of the binary process that the ions undergo in the observed plasma system. If the mean free path L is larger than the size of the whole plasma system, the width of the pre-sheath is determined by the size of the plasma container.[1,2] The function of the pre-sheath is to accelerate the positive ions in such a way that they fulfil the well-known Bohm criterion[3] at the boundary between the pre-sheath and the sheath called the sheath edge. The correct velocity of positive ions at the sheath edge is needed in order to adjust the positive space charge associated with the ions that are entering into the sheath. Usually, the sheath is collisionless and planar, and as already mentioned, its characteristic length scale λ_D is much smaller than the characteristic length scale L of the pre-sheath. In actual plasma, the ratio $\varepsilon = \lambda_D/L$ is usually very small but finite. Thus, it is logical to analyze the plasma boundary problem in these two scales separately. In the asymptotic two-scale limit $\varepsilon \to 0$, both scales are completely decoupled. On the sheath scale of this limit, the sheath edge is infinitely far from the wall, and the electric field at the sheath edge is zero.[4] On the pre-sheath scale of the asymptotic two-scale limit, the sheath is infinitesimally thin, and the electric field at the sheath edge is infinite. As can be seen, the sheath edge has an ambiguous behavior, and one has to remove the contradicting behavior by solving the matching problem.[5]

The role of ion temperature in the sheath formation is a hot topic, which is investigated extensively. Theoretically, fully self-consistent analysis of the influence of positive ion temperature to the plasma-wall transition would require a solution of a Tonks-Langmuir problem with a warm ion source,[6,7] which is far beyond the scope of this work. Satisfactory solutions of this problem have started to appear only recently, and it is not possible to give a review of relevant references in the Introduction like this one. So let us only mention that the current state of the art of solving the Tonks-Langmuir problem with a warm ion source can be found in Refs. 7 and 8 and many relevant references can be found in Ref. 8. It is, therefore, not surprising that the problem of the ion temperature effects to the plasma-sheath formation is still mainly studied with one dimensional

steady-state fluid models.[9–17] In these papers, the ions are treated with continuity and momentum exchange equation, while the Boltzmann relation is assumed for the electrons and also for negative ions if they are present in the plasma.[15,18] In the above mentioned papers, the closure is made by the assumption that the ions are isothermal and ideal gas law is used to eliminate the pressure gradient term from the momentum exchange equation. The ion temperature is treated as a given independent parameter. Some other authors[18–23] use a very similar approach, but they assume that the ion flow to the wall is adiabatic with a constant polytropic coefficient κ equal to 3, which corresponds to the one-dimensional adiabatic ion flow.

Attempts to develop a fluid model which would go to higher moments of the Boltzmann equation for ions than the momentum exchange equation are very rare. An interesting work was reported by Das *et al.*[24] where the plasma-wall transition in a non-magnetized plasma has been studied by a fluid model using the continuity, momentum transfer, and energy transfer equations for the ions, while the Boltzmann relation has been used for the electrons. In this sense, somewhat outstanding are 3 papers by Zawaideh and coworkers.[25–27] In the first paper, Zawaideh *et al.*[25] developed a truly impressive two-fluid model intended for the analysis of parallel transport in magnetized collisional plasma. The ions have been described by the equation of continuity, equation of motion, and two energy transport (pressure) equations—one for direction of magnetic field and the other for perpendicular direction. A similar set of equations was derived also for the electrons. In the next paper,[26] the model was developed further, and in the last paper of this "trilogy," a fully developed model was used for the analysis of the plasma sheath transition in a magnetized plasma with various degrees of collisionality. The set of equations in the last paper[27] consists of the equation of continuity (with zero source term), equation of motion, and two pressure equations (perpendicular and parallel with respect to magnetic field) for the ions, while the electrons are described by equation of continuity (with zero source term), equation of motion, pressure equation in the direction parallel to the magnetic field, and even energy flux equation—this means one additional moment of the Boltzmann equation. The main conclusion of this work is the following. Simpler models that use basically only the continuity equation and equation of motion predict solutions with monotonic potential profiles in the sheath for supersonic ion flows and oscillatory potential profiles for subsonic ion flows. But a more advanced set of equations used in Ref. 27 also predicts a third class of solutions. When the ion flow speed is between the ion thermal velocity ion sound velocity, solutions exist, where the electric field is positive definite and oscillatory, but the potential is monotonic. Two additional works deserve to be mentioned. The first is by Laux *et al.*[28] and the second by Gunn.[29] Laux and coworkers[28] extended Hutchinson's[30] model of a probe in a strongly magnetized plasma flow by adding the energy equation for ions, while electrons were assumed to obey the Boltzmann factor. Gunn[29] investigated the influence of a source of poloidal momentum on the collisionless tokamak scrape-off layer. He compared the solutions of the kinetic equation for ion flow and the corresponding system of fluid equations assuming zero ion heat flux. Both models agreed well for small poloidal Mach numbers of the momentum source. Gyergyek and Kovačič[31] have recently presented a steady state, one-dimensional, two-fluid model which was used for the analysis of the plasma-wall transition in front of a negative planar electrode. Continuity, momentum exchange, and energy transport equations have been used for the ions, while the continuity and momentum exchange equations have been used for the electrons. The model has been solved for zero ion temperature at the boundary, and some effects of variation of ε, Coulomb collisions between ions and electrons and charge exchange collisions between ions and neutrals have been examined. This work and Paper II[32] are a continuation of the work presented in Ref. 31. Attention is focused on the determination of the boundary conditions when non-zero ion temperatures at the boundary are selected.

In this paper, the model is solved for $\varepsilon > 0$ in the pre-sheath and in the sheath region simultaneously, while in Paper II,[32] the model is solved for $\varepsilon = 0$ in the pre-sheath and in the sheath scale separately. In Sec. II, the model developed in Ref. 31 is presented. In Sec. III, some results are shown. In Sec. IV, an attempt to include the divergence of the ion heat flux vector into the model is presented, and in Sec. V, the conclusions are given.

II. MODEL

Basic equations of a steady state, one dimensional, two fluid models have been derived in a recent paper by Gyergyek and Kovačič.[31] They can be written in two forms, depending on the normalization of the space coordinate x. If x is normalized to ionization length L, the model equations read[31]

$$\frac{d}{d\xi}(N_i V_i) = s_i, \tag{1}$$

$$\frac{d}{d\xi}(N_e V_e) = s_e, \tag{2}$$

$$P_i = N_i \Theta, \tag{3}$$

$$N_i V_i \frac{dV_i}{d\xi} = \eta N_i - \frac{dP_i}{d\xi} - Z_{CX} N_i V_i - V_i s_i, \tag{4}$$

$$\mu N_e V_e \frac{dV_e}{d\xi} = -\eta N_e - \frac{dN_e}{d\xi} - \mu V_e s_e, \tag{5}$$

$$\frac{1}{2} V_i \frac{dP_i}{d\xi} + \frac{3}{2} P_i \frac{dV_i}{d\xi} = Z_{CX} N_i V_i^2 + \frac{1}{2} V_i^2 s_i, \tag{6}$$

$$\eta = -\frac{d\Psi}{d\xi}, \tag{7}$$

$$\varepsilon^2 \frac{d^2\Psi}{d\xi^2} = N_e - N_i. \tag{8}$$

If on the other hand x is normalized to the Debye length λ_D, the system of equations gets the following form

$$\frac{d}{dX}(N_iV_i) = \varepsilon s_i, \tag{9}$$

$$\frac{d}{dX}(N_eV_e) = \varepsilon s_e, \tag{10}$$

$$P_i = N_i\Theta, \tag{11}$$

$$N_iV_i\frac{dV_i}{dX} = \chi N_i - \frac{dP_i}{dX} - \varepsilon[Z_{CX}N_iV_i + V_is_i], \tag{12}$$

$$\mu N_eV_e\frac{dV_e}{dX} = -\chi N_e - \frac{dN_e}{dX} - \varepsilon\mu V_es_e, \tag{13}$$

$$\frac{1}{2}V_i\frac{dP_i}{dX} + \frac{3}{2}P_i\frac{dV_i}{dX} = \varepsilon\left[Z_{CX}N_iV_i^2 + \frac{1}{2}V_i^2s_i\right], \tag{14}$$

$$\chi = -\frac{d\Psi}{dX}, \tag{15}$$

$$\frac{d^2\Psi}{dX^2} = N_e - N_i. \tag{16}$$

The following variables have been introduced:

$$\lambda_D = \sqrt{\frac{\varepsilon_0kT_e}{n_0e_0^2}}, \quad c_0 = \sqrt{\frac{kT_e}{m_i}}, \quad L = c_0\tau, \quad \varepsilon = \frac{\lambda_D}{L},$$
$$\mu = \frac{m_e}{m_i}, \quad \Theta = \frac{T_i}{T_e}, \quad N_i = \frac{n_i}{n_0}, \quad N_e = \frac{n_e}{n_0}, \quad V_i = \frac{u_i}{c_0},$$
$$V_e = \frac{u_e}{c_0}, \quad Z_{CX} = f_{CX}\tau, \quad \Psi = \frac{e_0\Phi}{kT_e}, \quad \xi = \frac{x}{L},$$
$$X = \frac{x}{\lambda_D}, \quad P_i = \frac{p_i}{p_0} = \frac{n_ikT_i}{n_0kT_e} = N_i\Theta. \tag{17}$$

Here, ε_0 is the permittivity of the free space, e_0 is the elementary charge, n_0 is the plasma density in the unperturbed region far away from the wall, k is the Boltzmann constant, T_e is the electron temperature, T_i is the ion temperature, m_e is the electron mass, m_i is the ion mass, n_i is the ion density, n_e is the electron density, τ is the ionization time (see below), u_i is the ion fluid velocity, u_e is the electron fluid velocity, Φ is the potential, and f_{CX} is the frequency of charge exchange collisions between the ions and neutral atoms of the same kind (see below).

Source terms for the ions and electrons $S_i(x)$ and $S_e(x)$ are modeled, based on the assumption that the main mechanism of ionization is ionizing collisions of electrons with neutral atoms. The source terms are given by

$$S_i(x) = S_e(x) = \frac{n_e(x)}{\tau}, \tag{18}$$

where τ must be understood as an effective ionization time, where losses of charged particles by recombination are already taken into account. In this model, since the electrons and singly charged positive ions are the only charged particles present in the plasma, it is clear that S_i and S_e must be equal. From Eqs. (17) and (18), it is easy to see that the dimensionless source terms s_i and s_e in Eqs. (1)–(14) are given by

$$s_i = s_e = N_e. \tag{19}$$

The only type of elastic collisions that are taken into account in this work is the charge exchange collisions between the ions and neutral atoms of the same kind. It is assumed that the ions, moving with the ion flow velocity u_i, collide with the neutral atoms that are at rest. The density of the "friction force" A_i that the ions experience because of those collisions is given by

$$A_i = -m_in_if_{CX}u_i. \tag{20}$$

Some authors[9,12] have assumed a more complicated collision term between ions and neutrals of the form $m_in_i(n_n\sigma(u_i)u_i)u_i$. Here, $\sigma(u_i)$ is the momentum transfer cross section for collisions between ions and neutrals, which is a function of ion velocity u_i, and n_n is the neutral gas density. The product $(n_n\sigma(u_i)u_i)$ gives the collision frequency, which depends on ion velocity u_i. In our model, the collision frequency f_{CX} is assumed to be a given constant. In the original model[31] also Coulomb collisions between ions and electrons were included. It was shown[31] that their effect is very small, so in this work, Coulomb collisions are not included.

The normalizing velocity c_0 is not the same as the ion sound velocity c_S, which is given by[31]

$$c_S = \sqrt{\frac{\kappa(x)kT_i(x) + kT_e}{m_i + m_e}}. \tag{21}$$

If Eqs. (17) and (21) are combined and the ion sound velocity is written in the dimensionless form

$$V_S = \frac{c_S}{c_0} = \sqrt{\frac{1 + \kappa\Theta}{1 + \mu}}. \tag{22}$$

Since the polytropic function κ and ion temperature T_i are space dependent, the ion sound velocity c_S is space dependent. The polytropic function is defined as[33,34]

$$\kappa = 1 + \frac{n_i}{T_i}\frac{dT_i}{dn_i} = 1 + \frac{N_i}{\Theta}\frac{d\Theta}{dN_i}. \tag{23}$$

The polytropic function gives the local value of the polytropic coefficient, which is equal to the ratio of the specific heats at constant pressure and at constant volume $\kappa = C_p/C_V$. In fluid models of the plasma-wall transition, it is usually assumed either $\kappa = 1$ for isothermal ion flow or $\kappa = 3$ for one-dimensional adiabatic ion flow. Only relatively recently it has been found[33] that in the plasma wall transition region, κ is not a constant, but it is space dependent. So, one speaks about the polytropic function instead of the polytropic coefficient.

III. RESULTS

The systems of Eqs. (1)–(8) and (9)–(16) are both systems of 8 ordinary differential equations for 8 unknown functions of ξ or X. Because both systems of equations are nonlinear, only numerical solutions can be found. For a unique solution, 8 boundary conditions must be specified. As we try to show in this work and in Part II[32] the correct determination of boundary conditions plays a very important role in the interpretation of results. Let us first take a look at one example of the solutions of the system (1)–(8) (Fig. 1) and one example of the solutions of the system (9)–(16) (Fig. 2). For the curves shown in Fig. 1,

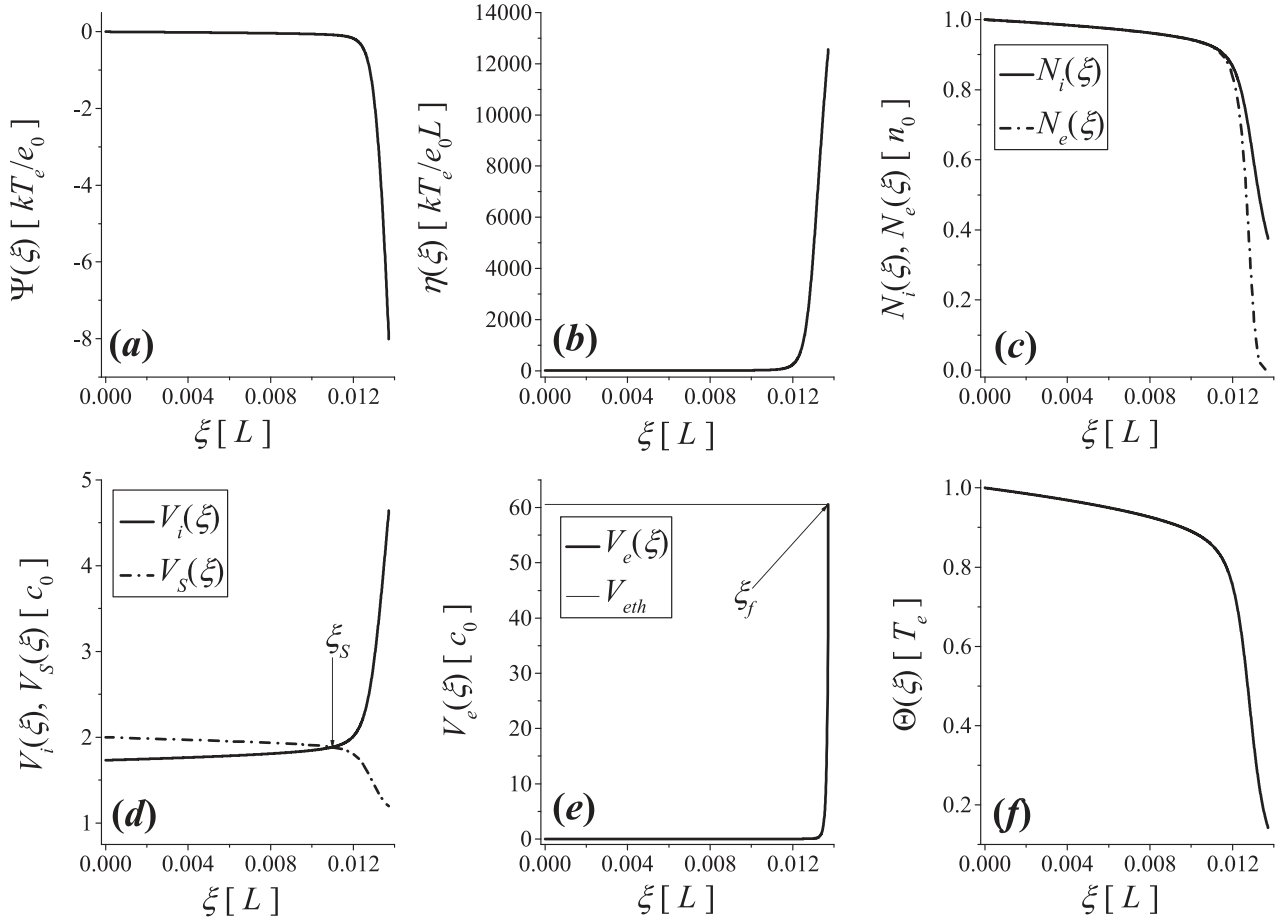

FIG. 1. Solutions of systems (1)–(8) for $\mu = 1/3670.482$, $Z_{CX} = 0$, $\varepsilon = 2 \times 10^{-4}$, $\Psi(0) = V_e(0) = 0$, $N_i(0) = N_e(0) = 1$, $\Theta(0) = P_i(0) = 1$, $V_i(0) = 1.73205081$, and $\eta(0) = 3.4641$.

the following parameters and boundary conditions are selected: $\mu = 1/3670.482$ (deuterium mass), $Z_{CX} = 0$ (no charge exchange collisions), $\varepsilon = 2 \times 10^{-4}$ (a realistically small ratio between the Debye and the ionization length), $\Psi(0) = V_e(0) = 0, N_i(0) = N_e(0) = 1, \Theta(0) = P_i(0) = 1, V_i(0) = 1.73205081$, and $\eta(0) = 3.4641$. Integration of the system (1)–(8) (Fig. 1) starts at $\xi = 0$ and proceeds in the positive direction of ξ. In plots (a), (b), and (c), potential $\Psi(\xi)$, electric field $\eta(\xi)$, and density $N_{ie}(\xi)$ profiles are displayed. Potential and both densities are monotonically decreasing functions of ξ, while the electric field increases monotonically. In plot (d), ion velocity $V_i(\xi)$ is shown together with the ion sound velocity $V_S(\xi)$. Vertical arrow marks their intersection, which occurs at $\xi = \xi_S$. Because at $\xi = \xi_S$ the Bohm criterion[3] is fulfilled in its marginal form ($V_i(\xi_S) = V_S(\xi_S)$), the coordinate ξ_S is identified as the sheath edge. In plot (e), the electron velocity profile $V_e(\xi)$ is shown. Velocity $V_e(\xi)$ is a monotonically increasing function of ξ, and when it reaches the electron thermal velocity V_{eth} (thin horizontal line), given the formula (24), the systems (1)–(8) become singular. The position of the singularity is labeled by ξ_f and $V_e(\xi_f) = V_{eth}$. The electron velocity $V_e(\xi)$ increases very slowly in the largest part of the solution domain. It increases very quickly if it is only very close to ξ_f. This can be understood easily. The source term in the continuity equation (2) is equal to the electron density, $s_e(\xi) = N_e(\xi)$ and is, therefore, positive everywhere. So, the electron flux $\Gamma_e(\xi) = N_e(\xi)V_e(\xi)$ is an increasing function of ξ. Since in the sheath (close to ξ_f) the electron density decreases quickly [plot (*c*)], the electron velocity must compensate this by a strong jump. Such sharp jump of electron flow velocity in the sheath has been observed also in particle-in-cell (PIC) simulations.[35] The ion temperature $\Theta(\xi)$, shown in plot (*f*), is a monotonically decreasing function of ξ.

In Fig. 2, solutions of systems (9)–(16) are presented for the same parameters and boundary conditions. The only difference is that the electric field at $X = 0$ is $\chi(0) = 6.9282 \times 10^{-4}$. One sees immediately that the solutions shown in both figures are identical; the only difference is in the scaling of the space coordinate and of the electric field. The positions of the sheath edge and of the singularity in Fig. 2 are labeled X_S and X_f, respectively. Since the solutions of the systems (1)–(8) and (9)–(16) for a finite ε are identical for the same parameters and boundary conditions, only systems (9)–(16) will be used for presentation of the results from now on. The reason is that scaling of the space coordinate with λ_D is more convenient for the graphical presentation of results.

The singularity points ξ_f and X_f are eigenvalues of the systems (1)–(8) and (9)–(16). The values of the solutions $\Psi(X_f)$, $\chi(X_f)$, etc., at the singularity point have no particular physical meaning. So, it is a bit problematic to call the distance $X_f - X_S$, the "sheath thickness" or to call the difference

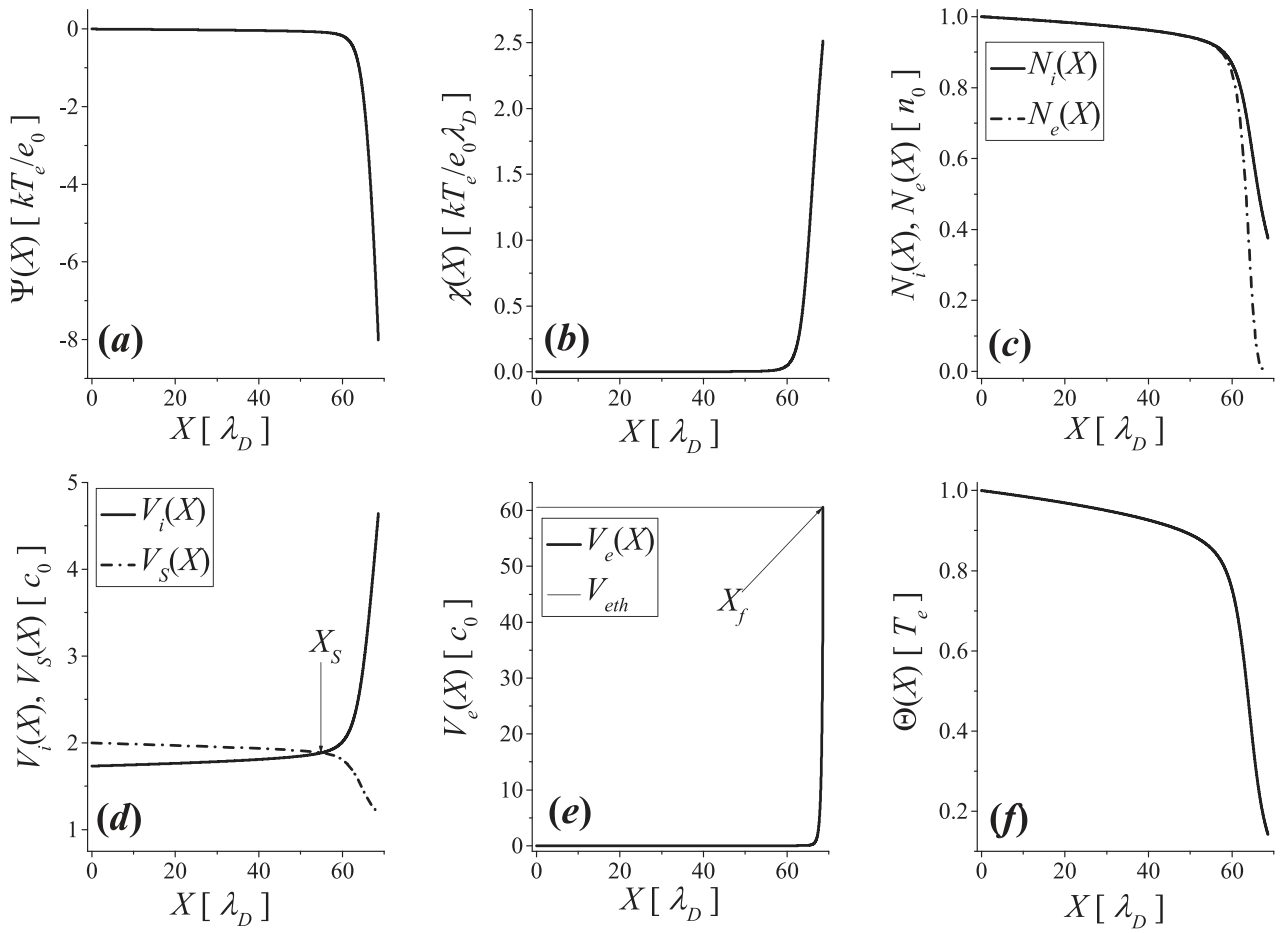

FIG. 2. Solutions of systems (9)–(16) for $\mu = 1/3670.482$, $Z_{CX} = 0$, $\varepsilon = 2 \times 10^{-4}$, $\Psi(0) = V_e(0) = 0, N_i(0) = N_e(0) = 1, \Theta(0) = P_i(0) = 1, V_i(0) = 1.73205081$, and $\chi(0) = 6.9282 \times 10^{-4}$.

$\Psi(X_S) - \Psi(X_f)$, the "sheath potential drop." Nevertheless, such terms will be used in the discussions below for practical purposes.

Next, an explanation of the boundary conditions should be given. The conditions $\Psi(0) = 0$ and $N_i(0) = N_e(0) = 1$ are easy to understand. The potential of the unperturbed plasma is set to zero. In addition, the unperturbed plasma is neutral, and it is natural to normalize the ion and electron density to unity. In our model, the temperature Θ is treated as a given, independent parameter, which is included in the model as a boundary condition $\Theta(0)$. The only limitation is that it must be positive. A few comments about the case $\Theta(0) = 0$ are given in Fig. 5. The ion pressure $P_i(0)$ must be consistent with $\Theta(0)$, $N_i(0)$ and Eq. (11).

Let us now focus on the ion velocity $V_i(0)$. It can be shown by a short calculation[31] that the systems of Eqs. (1)–(8) and (9)–(16) become singular if either the ion velocity V_i drops below the ion thermal velocity V_{ith} or the electron velocity V_e exceeds the electron thermal velocity V_{eth}. These thermal velocities are given by[31]

$$V_{ith} = \frac{1}{c_0}\sqrt{\frac{\kappa k T_i}{m_i}} = \sqrt{\kappa\Theta}, \quad V_{eth} = \frac{1}{c_0}\sqrt{\frac{kT_e}{m_e}} = \frac{1}{\sqrt{\mu}}. \tag{24}$$

As soon as $\Theta(0) > 0$ is selected, the ion velocity must be $V_i(0) \geq \sqrt{\kappa(0)\Theta(0)}$. Since $\kappa(0)$ can be found only after the system (9)–(16) has been solved [see formula (23)], one has to find $V_i(0)$ by a numerical trial and error method, which goes as follows. Initially, zero electric field $\chi(0) = 0$ and electron velocity $V_e(0) = 0$ are selected together with $\Psi(0) = 0$, $N_i(0) = N_e(0) = 1$, and the selected $\Theta(0)$, $P_i(0)$, μ, ε, and Z_{CX}. Then, some large enough value is selected for $V_i(0)$ and systems (9)–(16) are solved. If a singularity is encountered, $V_i(0)$ must be increased. If a physically acceptable monotonic solution is obtained, $V_i(0)$ is slightly decreased, and systems (9)–(16) are solved again. The goal is to find the minimum value $V_i(0)$ which still gives physically acceptable monotonic solutions of the system (9)–(16). When the minimum $V_i(0)$ is found, the electric field $\chi(0)$ is slightly increased. It turns out that at a larger electric field, the ion velocity $V_i(0)$ can be decreased further and monotonic solutions of systems (9)–(16) can still be found. In this way, $\chi(0)$ is gradually increased, while $V_i(0)$ is decreased. When a certain value of $\chi(0)$ is exceeded, physically acceptable solutions of systems (9)–(16) can be obtained only if $V_i(0)$ is increased and not decreased. The relationship between the values of $\chi(0)$ and $V_i(0)$ that give monotonic solutions of systems (9)–(16) is illustrated in Fig. 3. For the results presented in Fig. 3, the following parameters are selected: $\mu = 1/3670.482$, $Z_{CX} = 0$, and $\varepsilon = 2 \times 10^{-4}$. The following boundary conditions are selected: $\Psi(0) = 0$, $N_i(0) = N_e(0) = 1$, and $V_e(0) = 0$. Then, 4 values of

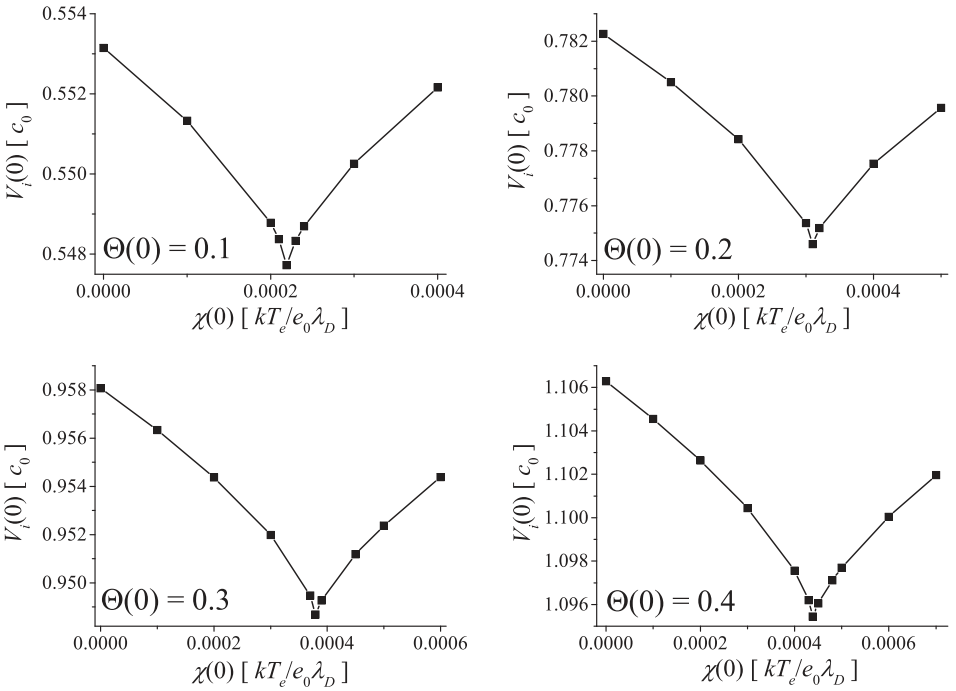

FIG. 3. Minimum ion velocity $V_i(0)$, which gives a monotonic solution of systems (9)–(16) versus $\chi(0)$.

$\Theta(0)$ are selected: $\Theta(0) = 0.1$, $\Theta(0) = 0.2$, $\Theta(0) = 0.3$, and $\Theta(0) = 0.4$. The values of $P_i(0)$ are selected accordingly. At each $\Theta(0)$, electric $\chi(0)$ and ion velocity $V_i(0)$ are gradually varied, as described earlier. The minimum ion velocity $V_i(0)$, which results in a monotonic solution of systems (9)–(16), is plotted versus the respective electric field $\chi(0)$. In this way, the graphs shown in Fig. 3 are obtained.

If systems (1)–(8) is solved instead of systems (9)–(16), the results are exactly the same; only $\eta(0)$ is rescaled with respect to $\chi(0)$ by the factor $\eta(0) = \chi(0)/\varepsilon = 5000\chi(0)$. The boundary conditions $\Theta(0)$, $V_i(0)$ and $\chi(0)$ [or $\eta(0)$] found by the method shown in Fig. 3 are called the "consistent boundary conditions." Further arguments related to the consistency of the boundary conditions $\Theta(0)$, $V_i(0)$, and $\eta(0)$ are presented in Part II,[32] where the system of Eqs. (1)–(8) is analyzed in the asymptotic two-scale limit and $\varepsilon = 0$ is inserted into Eqs. (1)–(8).

In Fig. 4, the relationship between the consistent boundary conditions $\Theta(0)$, $V_i(0)$, and $\chi(0)$ is illustrated further. The minimum ion velocity $V_i(0)$ (top graph) and the respective electric field $\chi(0)$ (middle plot), found by the method, described in Fig. 3, are shown versus $\Theta(0)$. The parameters $\mu = 1/3670.482$ and $\varepsilon = 2 \times 10^{-4}$ are the same as in Fig. 3. Also, the boundary conditions $\Psi(0) = V_e(0) = 0$, $N_i(0) = N_e(0) = 1$ are not changed. Two values of the frequency of the charge exchange collisions are selected: $Z_{CX} = 0$ and $Z_{CX} = 1$. It can be seen that the ion velocity $V_i(0)$ does not depend on Z_{CX}, but the electric field $\chi(0)$ does. If Z_{CX} is increased, $\chi(0)$ increases also. In the bottom plot $\chi(0)$ is plotted versus Z_{CX} for $\Theta(0) = 1$. It can be seen that the relation is linear.

By a simple fitting procedure performed in the top graph of Fig. 4, it is found that $V_i(0)$ and $\Theta(0)$ are related by

$$V_i(0) = \sqrt{3\Theta(0)}. \tag{25}$$

Factor 3 obviously corresponds to the "adiabatic" value of the polytropic function κ—see formula (24). As ion temperature $\Theta(0)$ is increased, the ion flow velocity $V_i(0)$ and electric field $\chi(0)$ or $\eta(0)$ must also be increased.

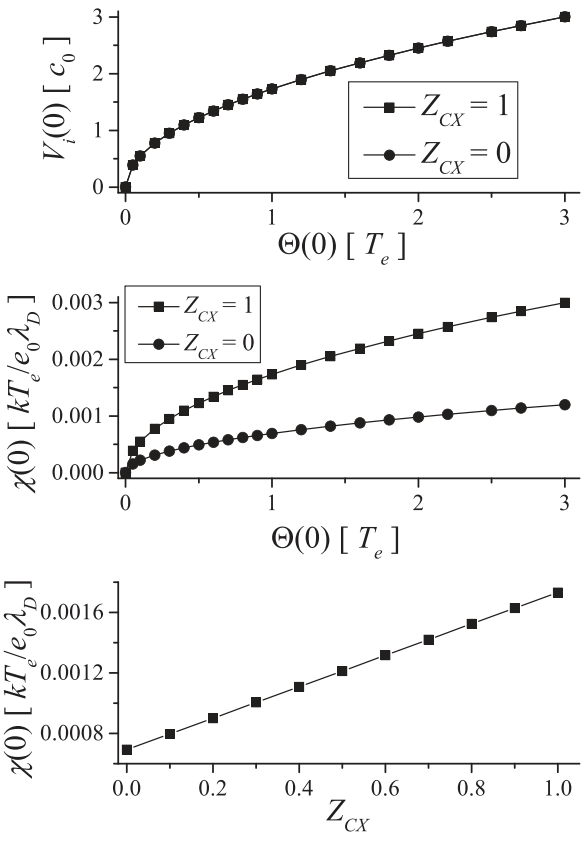

FIG. 4. In the top graph, the minimum ion velocity $V_i(0)$, which gives monotonic solution of the system (9)–(16), is plotted versus $\Theta(0)$ for 2 values of Z_{CX}. In the middle graph, the respective electric field $\chi(0)$ is shown versus $\Theta(0)$. In the bottom graph, the electric field $\chi(0)$ is plotted versus the frequency of charge exchange collisions Z_{CX} for $\Theta(0) = 1$.

Here, a remark about the selection of the zero ion temperature $\Theta(0) = 0$ is in order. From formula (25), one concludes that in this case $V_i(0) = 0$ should be selected and this would also imply $\chi(0) = 0$. But unfortunately, when $V_i(0) = 0$ is selected, this results in a singularity because of the division by zero in Eqs. (1) and (4) or (9) and (12). So, $V_i(0) > 0$ must be selected. But, in this case, the boundary conditions $\Theta(0) = 0$, $V_i(0) > 0$, and $\chi(0)$ or $\eta(0)$ cannot be found in a consistent way. It is, however, recommendable to select a small positive value of electric field $\chi(0)$ or $\eta(0)$.

The consistency of the boundary conditions $\Theta(0)$, $V_i(0)$, and $\chi(0)$ is illustrated in Fig. 5. In the top graphs (*a*), (*b*), and (*c*), the electric field $\chi(X)$, ion density $N_i(X)$, and ion velocity $V_i(X)$ are presented for the case, when zero ion temperature $\Theta(0) = 0$ is selected as a boundary condition. The selected parameters are as follows: $\mu = 1/3670.482$, $Z_{CX} = 0$, $\varepsilon = 2 \times 10^{-4}$, and boundary conditions are as follows: $\Psi(0) = V_e(0) = 0$, $N_i(0) = N_e(0) = 1$, and $V_i(0) = 5 \times 10^{-4}$. Two values of $\chi(0)$ are selected, $\chi(0) = 0$ and $\chi(0) = 3 \times 10^{-7}$. Thinner lines show the solutions of systems (9)–(16), which are found in the first electric field $\chi(0) = 0$. Solutions exhibit oscillations. Although their amplitude is not very large, they can become problematic, when the polytropic function κ is calculated, since the derivative $d\Theta/dN_i$ amplifies their effect strongly. Thicker line shows the solutions obtained when $\chi(0) = 3 \times 10^{-7}$ are selected. Oscillations are suppressed.

In the bottom plots (d), (e), and (f) the electric field $\chi(X)$, ion density $N_i(X)$, and ion velocity $V_i(X)$ are presented for the case when the ion temperature is $\Theta(0) = 0.2$. The parameters are the same as in the top plots: $\mu = 1/3670.482$, $Z_{CX} = 0$, and $\varepsilon = 2 \times 10^{-4}$. The boundary conditions are $\Psi(0) = V_e(0) = 0$ and $N_i(0) = N_e(0) = 1$. The thicker line shows the solution obtained with $\chi(0) = 3.09839 \times 10^{-4}$ and $V_i(0) = 0.774597$, while the thinner line shows the solution obtained with $\chi(0) = 3.0 \times 10^{-4}$ and $V_i(0) = 0.78$. Again, the solutions shown by thinner line exhibit the oscillations. Although such very precise determination of $\chi(0)$ and $V_i(0)$ is time consuming, it pays off when the polytropic function κ is calculated. One additional comment should be given. When $\Theta(0) > 0$ is selected, the corresponding $\chi(0)$ and $V_i(0)$ are uniquely determined by the method shown in Fig. 3. When $\Theta(0) = 0$ is selected, this is not the case since selection of $V_i(0)$ is rather arbitrary—it only has to be a small positive number. It turns out that to small values (like 10^{-6} or even 10^{-7}) are not the optimum choice because they can cause precision problems. Once $V_i(0)$ is selected, then the suitable electric field $\chi(0)$ (or $\eta(0)$) should be found in

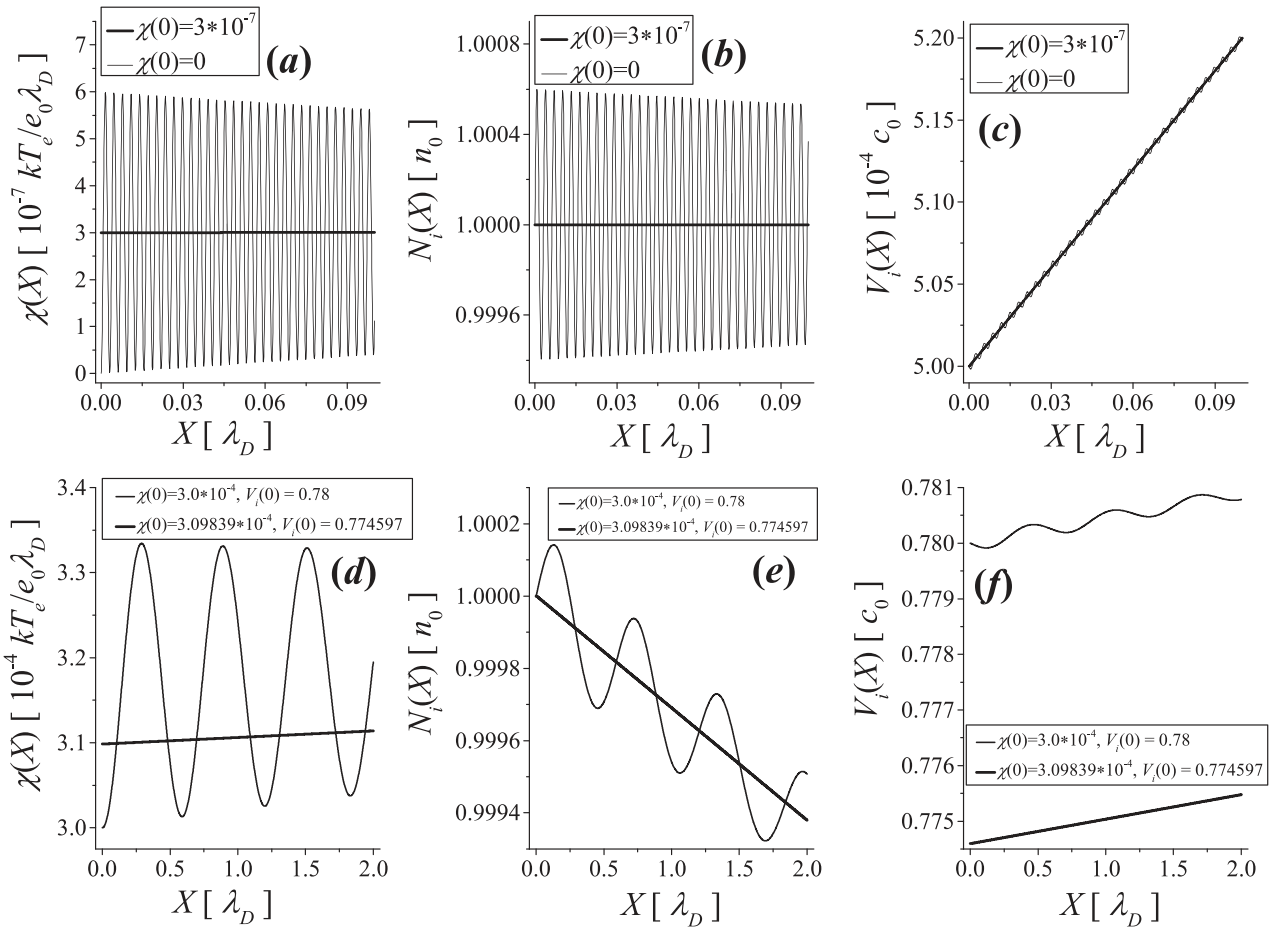

FIG. 5. In the top graphs (*a*), (*b*), and (*c*), the electric field $\chi(X)$, ion density $N_i(X)$, and ion velocity $V_i(X)$ are presented for the case when zero ion temperature $\Theta(0) = 0$ is selected. Thinner line shows the oscillating solution of systems (1)–(8), which is obtained, when $\chi(0) = 0$ is selected. Thicker line shows the solution found with $\chi(0) = 3 \times 10^{-7}$. In the bottom plots (d)–(f), the electric field $\chi(X)$, ion density $N_i(X)$, and ion velocity $V_i(X)$ are presented for the case, when the ion temperature is $\Theta(0) = 0.2$. The thicker line shows the solution obtained with $\chi(0) = 3.09839 \times 10^{-4}$ and $V_i(0) = 0.774597$, while the thinner line shows the oscillating solution obtained with $\chi(0) = 3.0 \times 10^{-4}$ and $V_i(0) = 0.78$.

such a way that the oscillatory behavior of the solutions is suppressed to the maximum extent possible. The optimum electric field is usually found by the trial and error method.

The last boundary condition that requires some explanation is the electron velocity $V_e(0)$. From the numerical point of view, any value between 0 and V_{eth} can be selected for $V_e(0)$. Physical arguments suggest the selection of one of the two most obvious choices. The first one is $V_e(0) = 0$. This boundary condition has been selected to get the results presented in Figs. 1–5 without any particular explanation. By selecting $V_e(0) = 0$, it is assumed that electron distribution function at $\xi = X = 0$ is perfectly symmetric Maxwellian and that there is no directed electron flow at $\xi = X = 0$. The second option is to select $V_e(0) = V_i(0)$, after $V_i(0)$ has been found by the method described in Fig. 3. In this way, it is assumed that at $\xi = X = 0$, there is no electric current in the plasma, since the ion and electron fluxes are equal. In Fig. 6, dependence of X_S, X_f, $\Psi(X_S), \Psi(X_f), \chi(X_S), \chi(X_f), N_i(X_S), N_i(X_f), V_i(X_S), V_i(X_f), V_e(X_S)\Theta(X_S)$, and $\Theta(X_f)$ on $V_e(0)$ is shown. The other parameters and boundary conditions are $\mu = 1/3670.482$, $Z_{CX} = 0$, $\varepsilon = 2 \cdot 10^{-4}$, $\Psi(0) = 0, N_i(0) = N_e(0) = 1, \Theta(0) = P_i(0) = 1, V_i(0) = 1.73205081$, and $\chi(0) = 6.9282 \times 10^{-4}$. It can be seen that the values at the sheath edge X_S, $\Psi(X_S)$, $\chi(X_S)$, $N_i(X_S)$, and $\Theta(X_S)$ are almost independent of $V_e(0)$. The electron velocity at the sheath edge $V_e(X_S)$ increases linearly with $V_e(0)$. The value at the sheath edge $V_e(X_S)$ is always only a little larger than the respective $V_e(0)$. The values at the singularity point X_f, $\Psi(X_f)$, $\chi(X_f)$, $N_i(X_f)$, $V_i(X_f)$, and $\Theta(X_f)$, on the other hand, are much more sensitive to $V_e(0)$. If $V_e(0)$ is increased, the potential, ion density, and ion temperature drop in the region between X_S and X_f all decrease, while the region $X_f - X_S$ becomes shorter.

In Figs. 7 and 8, the effects of selecting different $V_e(0)$ are illustrated further. In Fig. 7, solutions of systems (9)–(16) are shown for $\mu = 1/3670.482$, $\varepsilon = 2 \times 10^{-4}$, $Z_{CX} = 0$, $\Psi(0) = V_e(0) = 0$, $N_i(0) = N_e(0) = 1$, and 3 values of $\Theta(0)$: $\Theta(0) = 0.1$, $\Theta(0) = 0.2$, and $\Theta(0) = 0.3$. For each ion temperature $\Theta(0)$, the ion velocity $V_i(0)$ and electric field $\chi(0)$ are found using the method, described in Fig. 3. In plot (*a*), potential profiles are shown. When $\Theta(0)$ is increased, X_f decreases, but the absolute value $|\Psi(X_f)|$ increases. Electric field and positive space charge density in the sheath—shown in graphs (*b*) and (*c*)—also increase. In plot (*d*), the electron velocity profiles $V_e(X)$ are shown to illustrate the singularity $V_e(X_f) = V_{eth}$. Ion temperature profiles, shown in graph (*e*), reveal that $\Theta(X)$ is a monotonically decreasing function of X. In plot (*f*), the polytropic function $\kappa(X)$ is presented. Ion flow at the entrance of the system (at $X = 0$) is adiabatic. Because the electric field accelerates the ions towards the wall, the ions are expanding and cooling [plot (*e*)]. But the cooling is not so fast, as it would correspond to adiabatic expansion. The reason is that the ions receive some thermal energy from the electric field—see

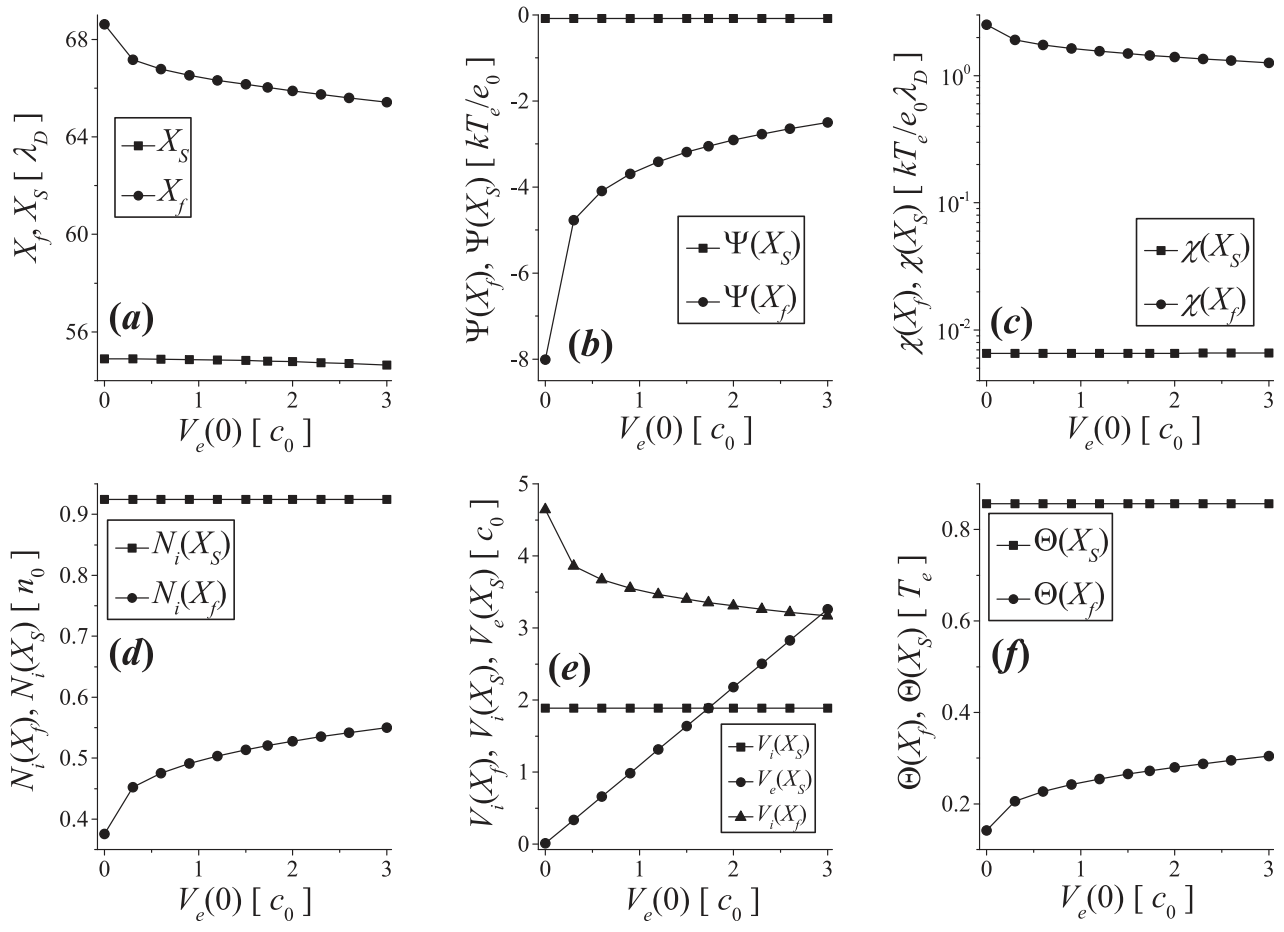

FIG. 6. Dependence of $X_S, X_f, \Psi(X_S), \Psi(X_f), \chi(X_S), \chi(X_f), N_i(X_S), N_i(X_f), V_i(X_S), V_i(X_f), V_e(X_S)\Theta(X_S)$, and $\Theta(X_f)$ on $V_e(0)$.

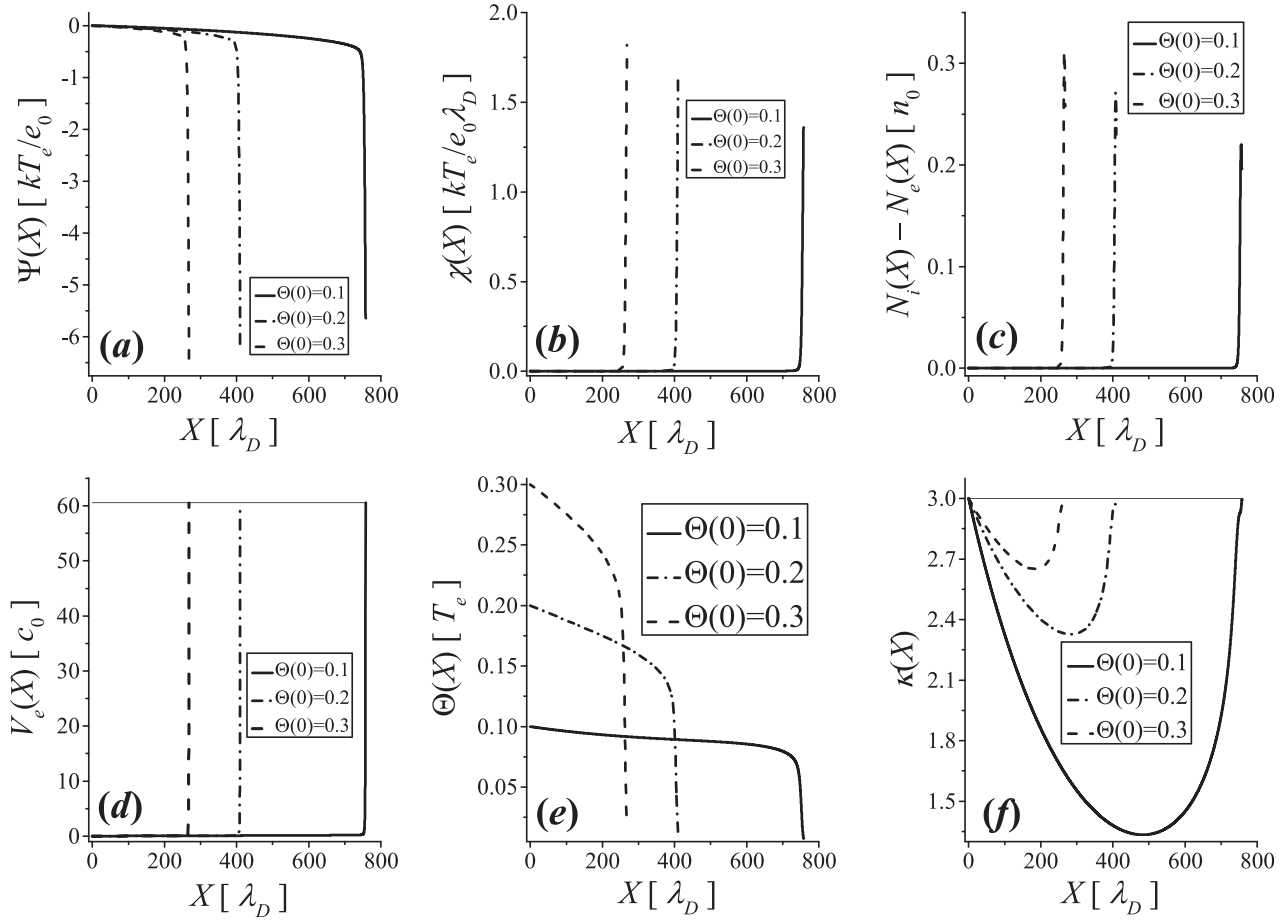

FIG. 7. Solutions of systems (9)–(16) for $\mu = 1/3670.482$, $\varepsilon = 2 \times 10^{-4}$, $Z_{CX} = 0$, $\Psi(0) = V_e(0)) = 0$, $N_i(0) = N_e(0) = 1$, $V_i(0) = \sqrt{3\Theta(0)}$, and 3 values of $\Theta(0)$: $\Theta(0) = 0.1$, $\Theta(0) = 0.2$, and $\Theta(0) = 0.3$.

also discussion below—Fig. 9. So, $\kappa(X)$ at first decreases, reaches a minimum, and then increases. Close to X_f the value of κ is again very close to 3.

Very similar results are shown in Fig. 8. Also, in this figure, the solutions of systems (9)–(16) are shown. The parameters and boundary conditions are almost the same, as in Fig. 7: $\mu = 1/3670.482$, $\varepsilon = 2 \times 10^{-4}$, $Z_{CX} = 0$, $\Psi(0) = 0$, $N_i(0) = N_e(0) = 1$, and same 3 values of $\Theta(0)$: $\Theta(0) = 0.1, \Theta(0) = 0.2$, and $\Theta(0) = 0.3$. For each ion temperature $\Theta(0)$, the ion velocity $V_i(0)$ and electric field $\chi(0)$ are found using the method, described in Fig. 3. The only difference is that this time, the boundary condition $V_e(0) = V_i(0)$ is selected. In Fig. 8, the absolute value $|\Psi(X_f)|$ decreases when $\Theta(0)$ is increased, while the electric field and positive space charge density still increase. The profiles of $\Theta(X)$ and $\kappa(X)$ shown in Figs. 7 and 8 cannot be distinguished. The boundary condition $V_e(0)$ has a very little or no effect on ion heating and cooling in the plasma-wall transition region. It also has no effect to the "self-consistent" boundary conditions $V_i(0)$ and $\chi(0)$.

In Figs. 9 and 10, two mechanisms of ion heating in the plasma wall transition region are illustrated. In Fig. 9, the solutions of the system (9)–(16) are shown for $\mu = 1/3670.482$, $\varepsilon = 2 \times 10^{-4}$, $Z_{CX} = 0$, $\Psi(0) = V_e(0) = 0$, $N_i(0) = N_e(0) = 1$, and 3 values of $\Theta(0)$: $\Theta(0) = 0.01, \Theta(0) = 0.02$, and $\Theta(0) = 0.03$. For each ion temperature $\Theta(0)$, the ion velocity $V_i(0)$ and electric field $\chi(0)$ are found using the method, described in Fig. 3. In plots (a), (b), and (c), very similar results, as in Fig. 7, can be seen. As $\Theta(0)$ is increased, X_f decreases, while the absolute value of the potential at the singularity point $|\Psi(X_f)|$, electric field, and positive space charge density in the sheath all increase. Note that $\Theta(0)$ is 10 times smaller than in Fig. 7, while X_f is approximately 2 times larger. Let us focus on plots (*e*) and (*f*), where $\Theta(X)$ and $\kappa(X)$ are presented. At $X = 0$, the ion temperature has the prescribed value $\Theta(0)$, which close to the coordinate origin first slightly decreases, but then starts to increase, until it reaches a maximum and then rapidly decreases. Very similar temperature profiles have been observed also in Ref. 31, where it was assumed that the ions are born cold $\Theta(0) = 0$ and also in the kinetic model[33] and particle-in-cell simulations.[34] It is interesting that there is even a very good quantitative matching of the maximum ion temperature between this work and Refs. 33 and 34. In all cases, the maximum ion temperature is around 6 percent of the electron temperature.

The heating mechanism has been explained in Refs. 33 and 34 and also Ref. 31, so it will be described here only very briefly. The ions that are born at rest or with very small velocity (because their temperature is so low) are accelerated in the positive direction of X, towards the wall, by the electric field. So, at a certain position X_1, where the potential is Ψ_1, their velocity is very close to $\sqrt{-2\Psi_1}$. Since new very

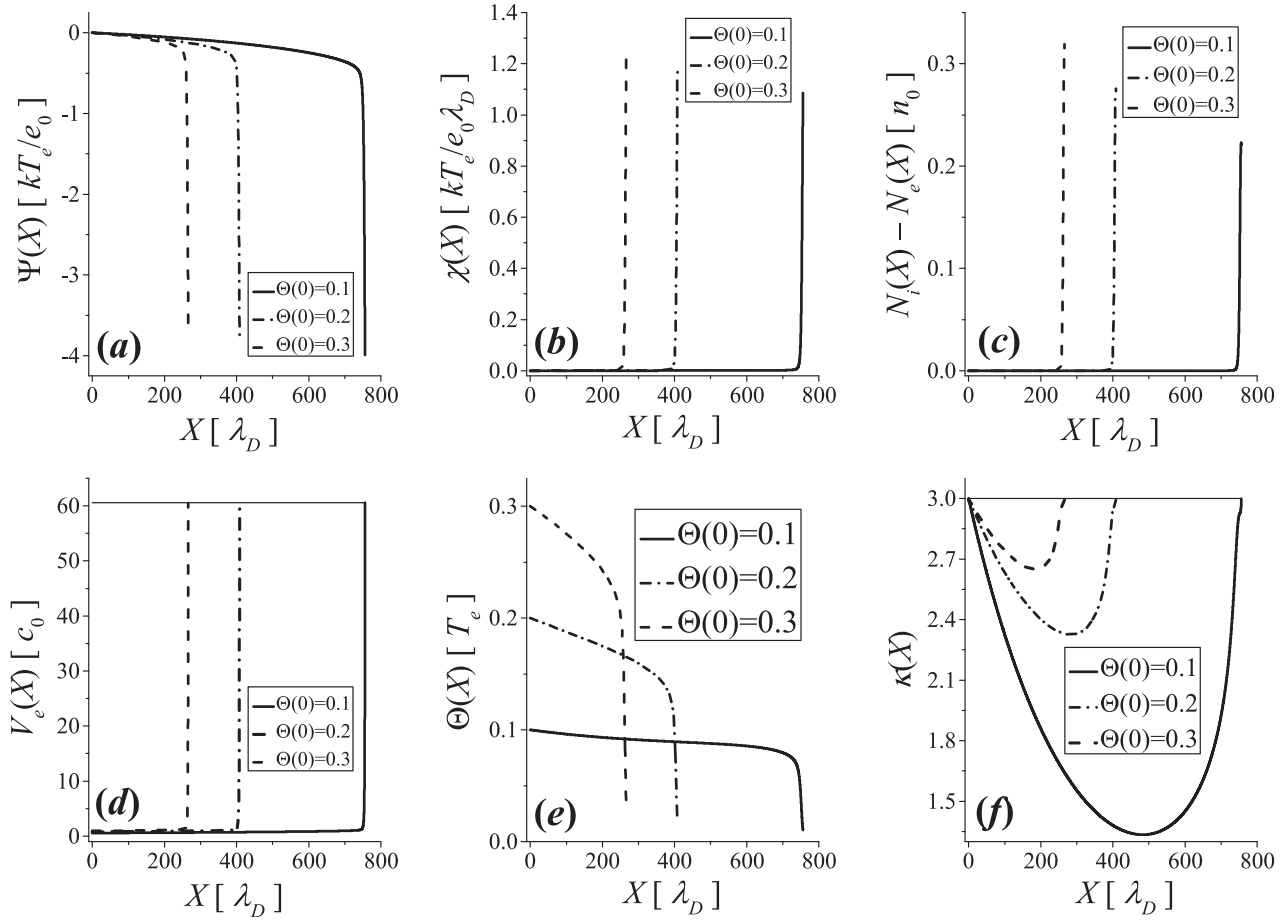

FIG. 8. Solutions of systems (9)–(16) for $\mu = 1/3670.482$, $\varepsilon = 2 \times 10^{-4}$, $Z_{CX} = 0$, $\Psi(0) = 0$, $V_e(0) = V_i(0) = \sqrt{3\Theta(0)}$, $N_i(0) = N_e(0) = 1$, and 3 values of $\Theta(0)$: $\Theta(0) = 0.1$, $\Theta(0) = 0.2$, and $\Theta(0) = 0.3$.

slow ions are also born everywhere in the system, the ion distribution function obtains a shape, which has a cutoff velocity very close to $\sqrt{-2\Psi_1}$, but it is also populated in the low velocity part. As X increases, $\sqrt{-2\Psi(X)}$ also increases and the ion distribution function becomes wider, which means larger ion temperature. In more thermodynamic terms, one could say that the electric field energy is converted into ion thermal energy. But close to the sheath edge, the electric field becomes larger, while the birth rate of new slow ions decreases, because $N_e(X)$ decreases. So, the ion distribution function becomes depleted in the low velocity part and therefore becomes more narrow. This also means smaller ion temperature. When the electric field becomes large enough, the electric field energy is converted into kinetic energy of the ion beam.[33] This explains the strong drop of ion temperature close to X_f. The profile $\kappa(X)$, shown in plot (*f*), is consistent with such scenario. The ion flow at the entrance into the system (at $X = 0$) is adiabatic, but then κ decreases rapidly and even becomes negative. A negative value of κ indicates that the ions are expanding and heating at the same time.[33] As X increases, heating of the ions becomes weaker and $\kappa(X)$ increases. Close to X_f, the ion flow again becomes adiabatic and κ reaches values very close to 3.

In Fig. 10, an illustration of the effect of charge exchange collisions is presented. In this figure, solutions of systems (9)–(16) are shown for $\mu = 1/3670.482$, $\varepsilon = 2 \times 10^{-4}$, $Z_{CX} = 1$, $\Psi(0) = V_e(0) = 0$, $N_i(0) = N_e(0) = 1$, and 3 values of $\Theta(0)$: $\Theta(0) = 0.1$, $\Theta(0) = 0.2$, and $\Theta(0) = 0.3$. For each ion temperature $\Theta(0)$, the ion velocity $V_i(0)$ and electric field $\chi(0)$ are found using the method described in Fig. 3. Results shown in plots (a), (b), and (c) are very similar to those shown in Figs. 7–9: when $\Theta(0)$ is increased, X_f decreases, while the absolute value of the potential at the singularity point $|\Psi(X_f)|$, electric field, and positive space charge density in the sheath all increase. The electron velocity profiles $V_e(X)$ are shown in plot (*d*) to indicate the position of the singularity X_f. In plot (*e*), ion temperature profiles $\Theta(X)$ are displayed. The lowest selected temperature $\Theta(0) = 0.1$ starts to increase immediately. The temperature increases until a maximum is reached close to the sheath edge and then a rapid cooling of ions follows. The charge exchange collisions are the additional heating mechanism for the ions. This was also found in Ref. 33. The corresponding polytropic function $\kappa(X)$, shown in plot (*f*), starts with a negative value, then increases, reaches a maximum close to the sheath edge and then decreases. Negative κ is an indication that the ions are expanding and heating at the same time. When $\Theta(0) = 0.2$ is selected, ion temperature at first remains constant and then starts to decrease. Note that $\kappa(0) = 1$ in plot (*f*) is consistent with the isothermal ion flow. Finally, at $\Theta(0) = 0.3$, the ion temperature is a

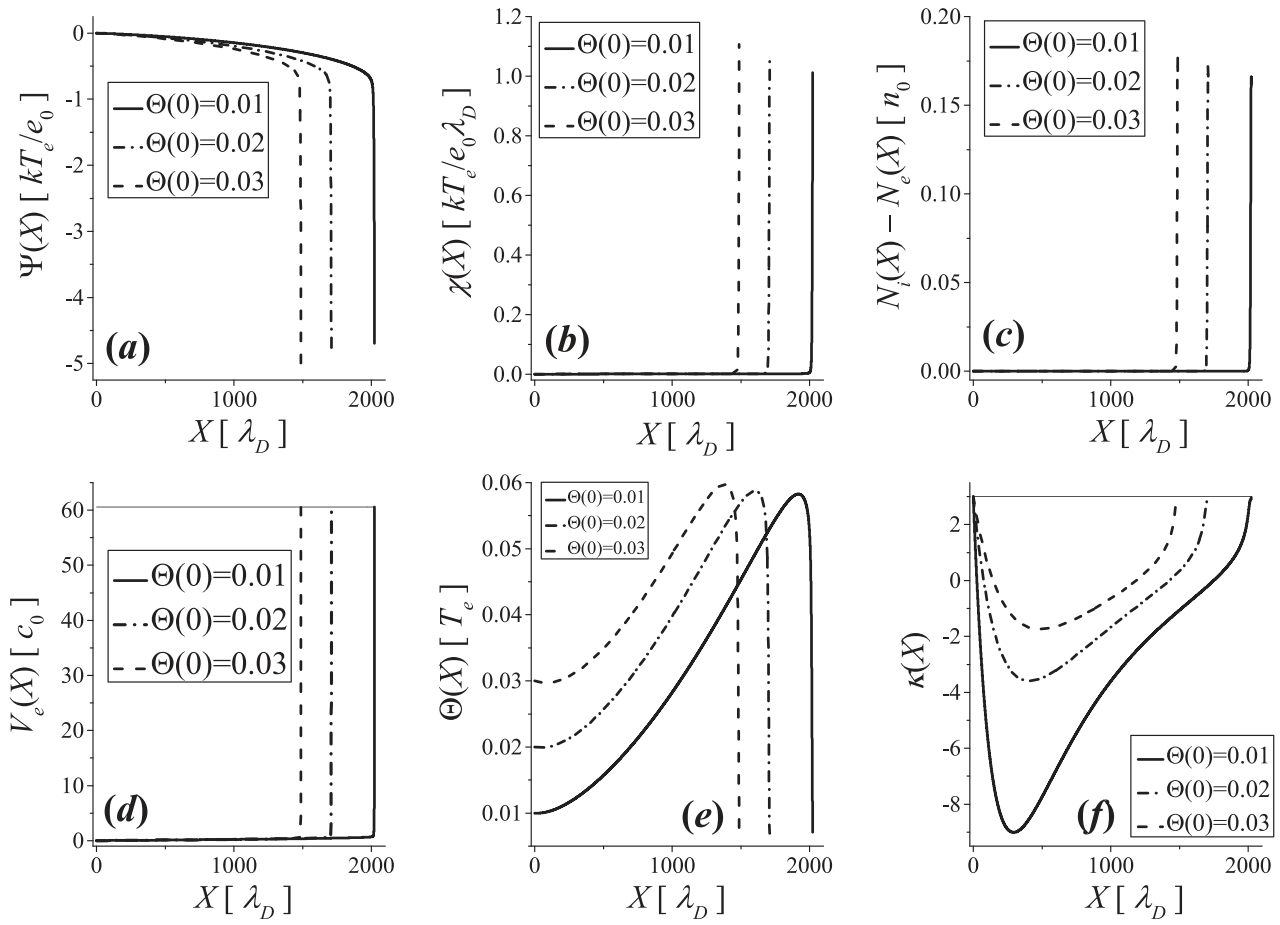

FIG. 9. Solutions of systems (9)–(16) for $\mu = 1/3670.482$, $\varepsilon = 2 \times 10^{-4}$, $Z_{CX} = 1$, $\Psi(0) = V_e(0)) = 0$, $N_i(0) = N_e(0) = 1$, and 3 values of $\Theta(0)$: $\Theta(0) = 0.1$, $\Theta(0) = 0.2$, and $\Theta(0) = 0.3$.

monotonically decreasing function of X. The corresponding values of κ are between 1.5 and 3. This indicates that the ions are cooling during their expansion, but the cooling is not adiabatic because they receive thermal energy from the electric field and from neutral particles through charge exchange collisions.

Presentation of results is concluded by a summary of ion temperature effects to the plasma wall transition region, which is shown in Figs. 11–13. For the results shown in Fig. 11, the following parameters are selected: $\mu = 1/3670.482$, $\varepsilon = 2 \times 10^{-4}$, and $Z_{CX} = 0$. The following boundary conditions are selected: $\Psi(0) = V_e(0) = 0$ and $N_i(0) = N_e(0) = 1$. The ion temperature $\Theta(0)$ is gradually increased. At each $\Theta(0)$, the ion velocity $V_i(0)$ and electric field $\chi(0)$ are found by the method, shown in Fig. 3 and systems (9)–(16) is solved. In plot (*a*), the positions X_S of the sheath edge and X_f of the singularity are plotted versus $\Theta(0)$. The vertical axis is shown in logarithmic scale, because X_S and X_f decrease for more than 2 orders of magnitude when $\Theta(0)$ is increased from 0 to 3. In plot (*b*), the "sheath thickness" $X_f - X_S$ is shown versus $\Theta(0)$. Plot (*b*) reveals that the sheath thickness decreases with increasing $\Theta(0)$. Obviously, the logarithmic scale in plot (*a*) can be deceiving. In graph (*c*), the electron velocity $V_e(X_S)$ at the sheath edge is plotted versus $\Theta(0)$. The scale on the vertical axis is logarithmic, since $V_e(X_S)$ decreases for more than 2 orders of magnitude when $\Theta(0)$ is increased from 0 to 3. In graph (*d*), the potentials at the sheath edge $\Psi(X_S)$ and at the singularity point $\Psi(X_f)$ are shown versus $\Theta(0)$. The sheath edge potential $\Psi(X_S)$ increases with increasing $\Theta(0)$ and it approaches to zero. The potential at the singularity point $\Psi(X_f)$, on the other hand, decreases with increasing $\Theta(0)$, but the absolute value $|\Psi(X_f)|$ increases. As a consequence, the "sheath potential drop" $\Psi(X_S) - \Psi(X_f)$ also increases with increasing $\Theta(0)$. By comparing graphs (*c*) and (*e*) and by looking at Fig. 6, one realizes that the sheath potential drop $\Psi(X_S) - \Psi(X_f)$ increases when the electron velocity at the sheath edge $V_e(X_S)$ decreases. If $V_e(0) = 0$ is selected, then $V_e(X_S)$ decreases with increasing ion temperature $\Theta(0)$. So, larger $\Theta(0)$ indeed results in better shielding of the plasma from the electrode as stated in Ref. 21. But, as shown in Fig. 7, this also depends on the boundary condition $V_e(0)$. Finally, in plot (*f*), the electric field at the sheath edge $\chi(X_S)$ is shown versus $\Theta(0)$. It has a maximum at approximately $\Theta(0) \approx 0.1$ and then decreases with increasing $\Theta(0)$. The values of the electric field at the sheath edge $\chi(X_S)$ are roughly 3 orders of magnitude smaller than the respective values $\chi(X_f)$ at the singularity point—see Figs. 2 and 7–10.

For the results shown in Fig. 12, the same parameters as in Fig. 11 are selected: $\mu = 1/3670.482$, $\varepsilon = 2 \times 10^{-4}$, and $Z_{CX} = 0$. Also, the boundary conditions are almost the same: $\Psi(0) = 0$ and $N_i(0) = N_e(0) = 1$. The ion temperature $\Theta(0)$

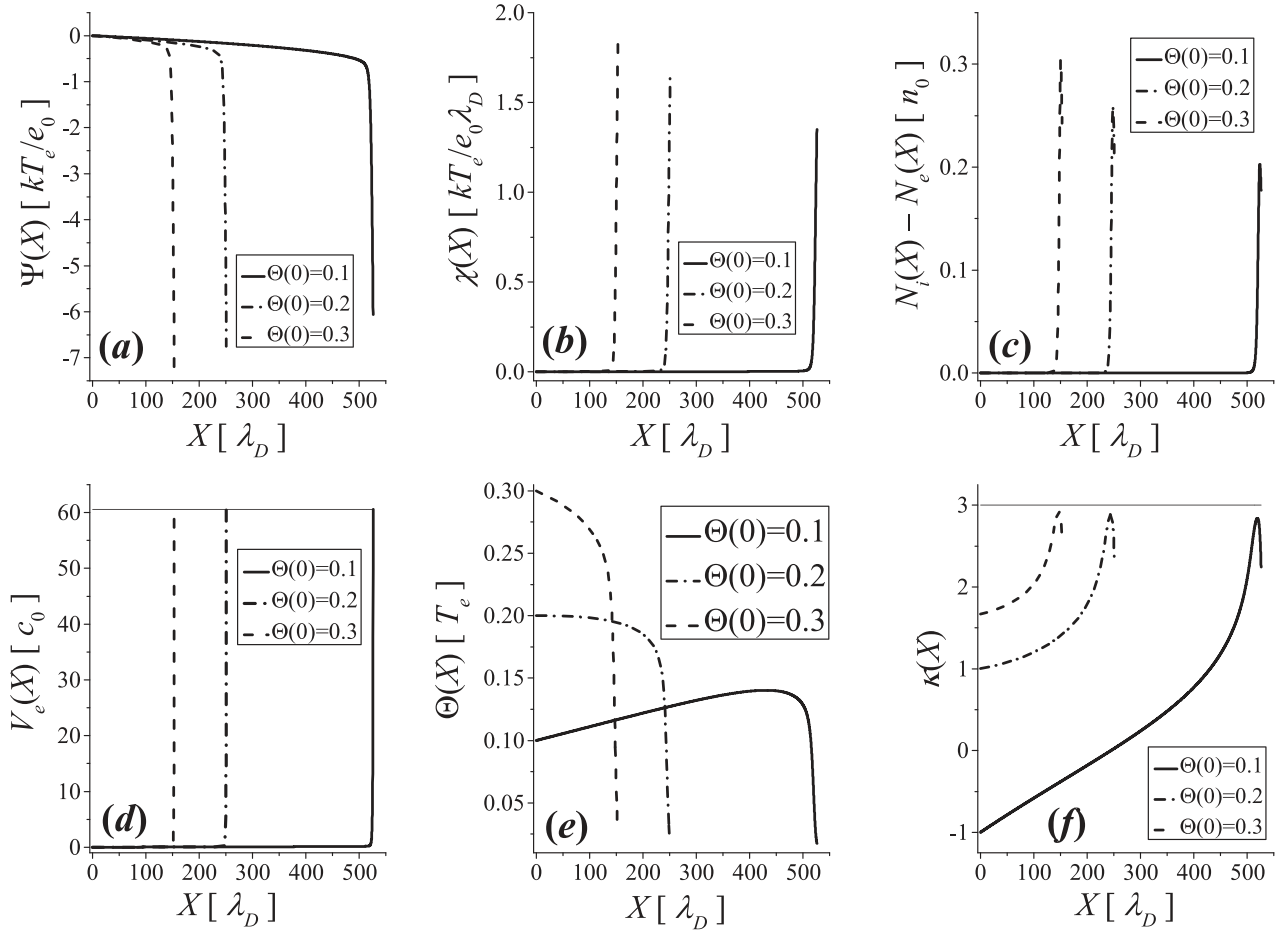

FIG. 10. Solutions of systems (9)–(16) for $\mu = 1/3670.482$, $\varepsilon = 2 \times 10^{-4}$, $Z_{CX} = 1$, $\Psi(0) = V_e(0) = 0$, $N_i(0) = N_e(0) = 1$, and 3 values of $\Theta(0)$: $\Theta(0) = 0.1$, $\Theta(0) = 0.2$, and $\Theta(0) = 0.3$.

is gradually increased. The only difference is the electron velocity $V_e(0)$. At each $\Theta(0)$, the ion velocity $V_i(0)$ and electric field $\chi(0)$ are found by the method shown in Fig. 3, and then, the boundary condition $V_e(0) = V_i(0)$ is selected. Then, systems (9)–(16) are solved. In plot (*a*), the positions X_S of the sheath edge and X_f of the singularity are plotted versus $\Theta(0)$. The vertical axis is shown in the logarithmic scale, because X_S and X_f decrease for more than 2 orders of

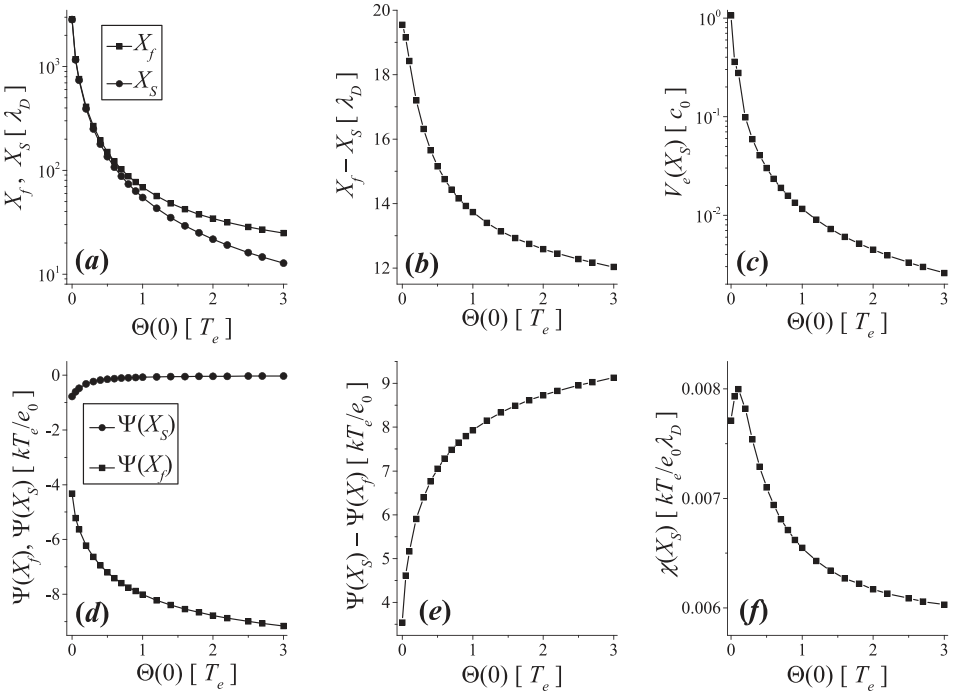

FIG. 11. Singularity point X_f and sheath edge position X_S plot (*a*), "sheath thickness" $X_f - X_S$—graph (b), electron velocity at the sheath edge $V_e(X_S)$—(c), potentials at the singularity point and at the sheath edge $\Psi(X_f)$ and $\Psi(X_S)$—(d), "sheath potential drop" $\Psi(X_S) - \Psi(X_f)$—(e) and electric field at the sheath edge $\chi(X_S)$—plot (f), versus $\Theta(0)$, when the boundary condition $V_e(0) = 0$ is selected.

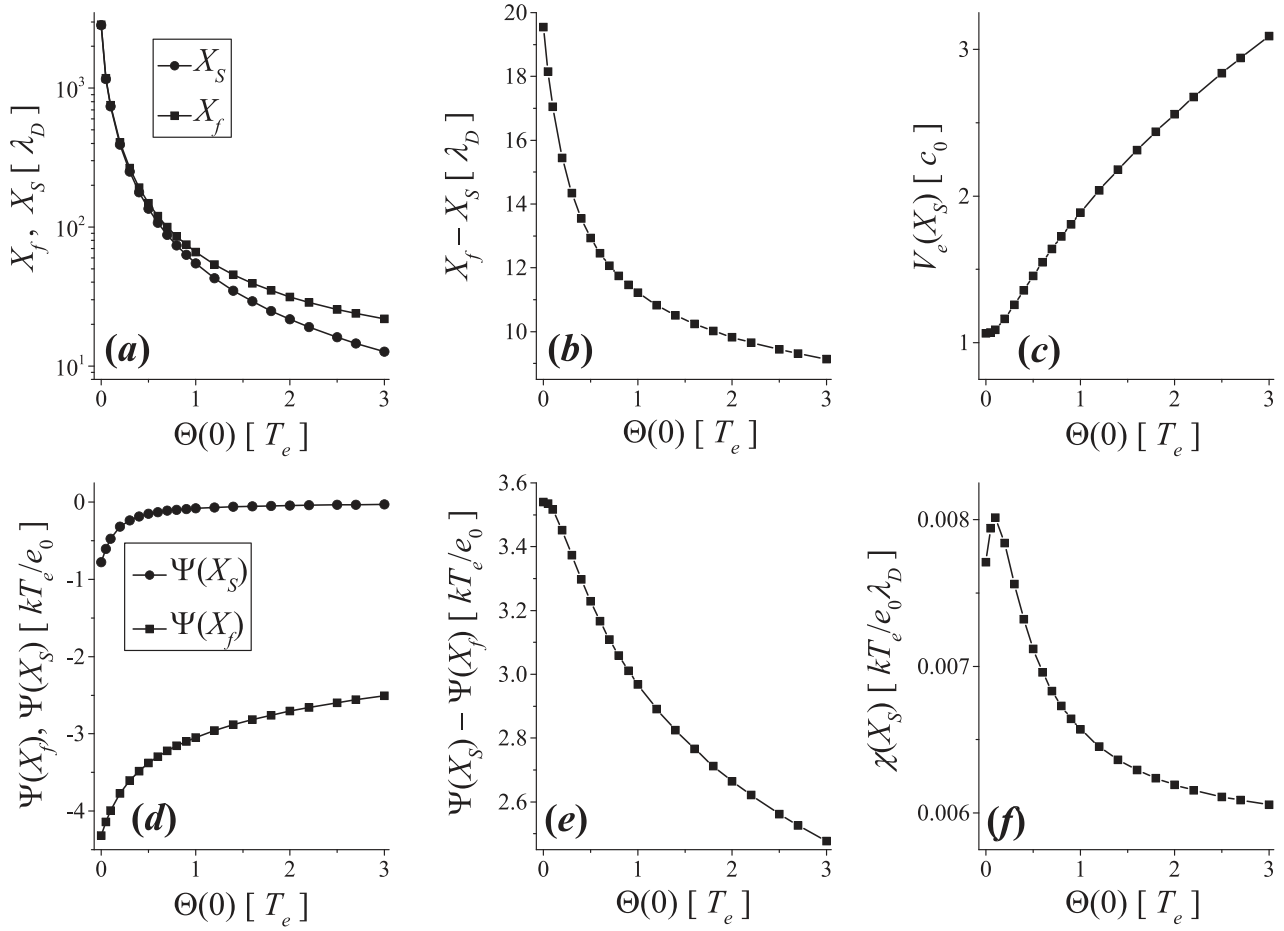

FIG. 12. Singularity point X_f and sheath edge position X_S plot (a), "sheath thickness" $X_f - X_S$—graph (b), electron velocity at the sheath edge $V_e(X_S)$—(c), potentials at the singularity point and at the sheath edge $\Psi(X_f)$ and $\Psi(X_S)$—plot (d), "sheath potential drop" $\Psi(X_S) - \Psi(X_f)$—(e) and electric field at the sheath edge $\chi(X_S)$—plot (f), versus $\Theta(0)$, when the boundary condition $V_e(0) = V_i(0)$ is used.

magnitude when $\Theta(0)$ is increased from 0 to 3. In plot (b), the "sheath thickness" $X_f - X_S$ is shown versus $\Theta(0)$. The results shown in plots (a) and (b) in Figs. 11 and 12 are very similar. The only difference between them is that at larger ion temperatures the decrease in the sheath thickness is stronger at $V_e(0) = V_i(0)$ than at $V_e(0) = 0$. In Fig. 12(c), the electron velocity at the sheath edge $V_e(X_S)$ is plotted versus $\Theta(0)$. It is only slightly larger than the respective ion and ion sound velocity at the sheath edge $V_S(X_S) = V_i(X_S)$. Such result can be understood easily. Both continuity Eqs. (9) and (10) require that the ion flux $\Gamma_i(X) = N_i(X)V_i(X)$ and the electron flux $\Gamma_e(X) = N_e(X)V_e(X)$ have the same derivative everywhere between $X = 0$ and $X = X_f$. If in addition $\Gamma_i(0) = \Gamma_e(0)$, then the functions $\Gamma_i(X)$ and $\Gamma_e(X)$ are equal everywhere. Because $\varepsilon > 0$, the ion density at the sheath edge $N_i(X_S)$ is not equal to the electron density at the sheath edge $N_e(X_S)$, but slightly larger. In order to maintain $\Gamma_i(X_S) = \Gamma_e(X_S)$, the electron velocity at the sheath edge $V_e(X_S)$ must be slightly larger than the respective ion velocities $V_S(X_S) = V_i(X_S)$ at the sheath edge. The consequence of this relatively large electron velocity at the sheath edge can be seen in plots (*d*) and (*e*). In (d), the potentials at the sheath edge $\Psi(X_S)$ and at the singularity point $\Psi(X_f)$ are shown versus $\Theta(0)$. The sheath edge potential $\Psi(X_S)$ increases with $\Theta(0)$ increasing and it approaches to zero. This result is almost identical to the respective result shown in Fig. 11(d). The potential at the singularity point $\Psi(X_f)$ increases (the absolute value $|\Psi(X_f)|$ decreases) with $\Theta(0)$ increasing, and consequently, the "sheath potential drop" $\Psi(X_S) - \Psi(X_f)$ decreases with increasing $\Theta(0)$. The difference between plots (*d*) and (*e*) in Figs. 11 and 12 is very obvious. Finally, in plot (*f*), the electric field at the sheath edge is shown versus $\Theta(0)$. It has a maximum at approximately $\Theta(0) \approx 0.1$ and then decreases with increasing $\Theta(0)$. Any differences between both plots (*f*) in Figs. 11 and 12 are very hard to find.

In Fig. 13, the ion densities $N_i(X_S)$ and $N_i(X_f)$ and temperatures $\Theta(X_S)$ and $\Theta(X_f)$ at the sheath edge at the singularity are displayed versus $\Theta(0)$. Parameters and boundary conditions are the same as in Figs. 11 and 12: $\mu = 1/3670.482$, $\varepsilon = 2 \times 10^{-4}$, $Z_{CX} = 0$, $\Psi(0) = 0$, and $N_i(0) = N_e(0) = 1$. In plots (*a*) and (*d*), $V_e(0) = 0$ is selected, while in graphs (*b*) and (*e*), $V_e(0) = V_i(0)$ is used. In (c) and (f), the differences $N_i(X_S) - N_i(X_f)$ and $\Theta(X_S) - \Theta(X_f)$ are shown versus $\Theta(0)$ for both choices $V_e(0) = 0$ and $V_e(0) = V_i(0)$. If the ion densities at the sheath edge $N_i(X_S)$ in graphs (*a*) and (*b*) are compared, it can be seen that they are almost identical. But the ion densities at the singularity $N_i(X_f)$ in plot (*b*) are considerably larger than in plot (*a*). Smaller "sheath potential drop" which is a consequence of a larger electron velocity at the sheath

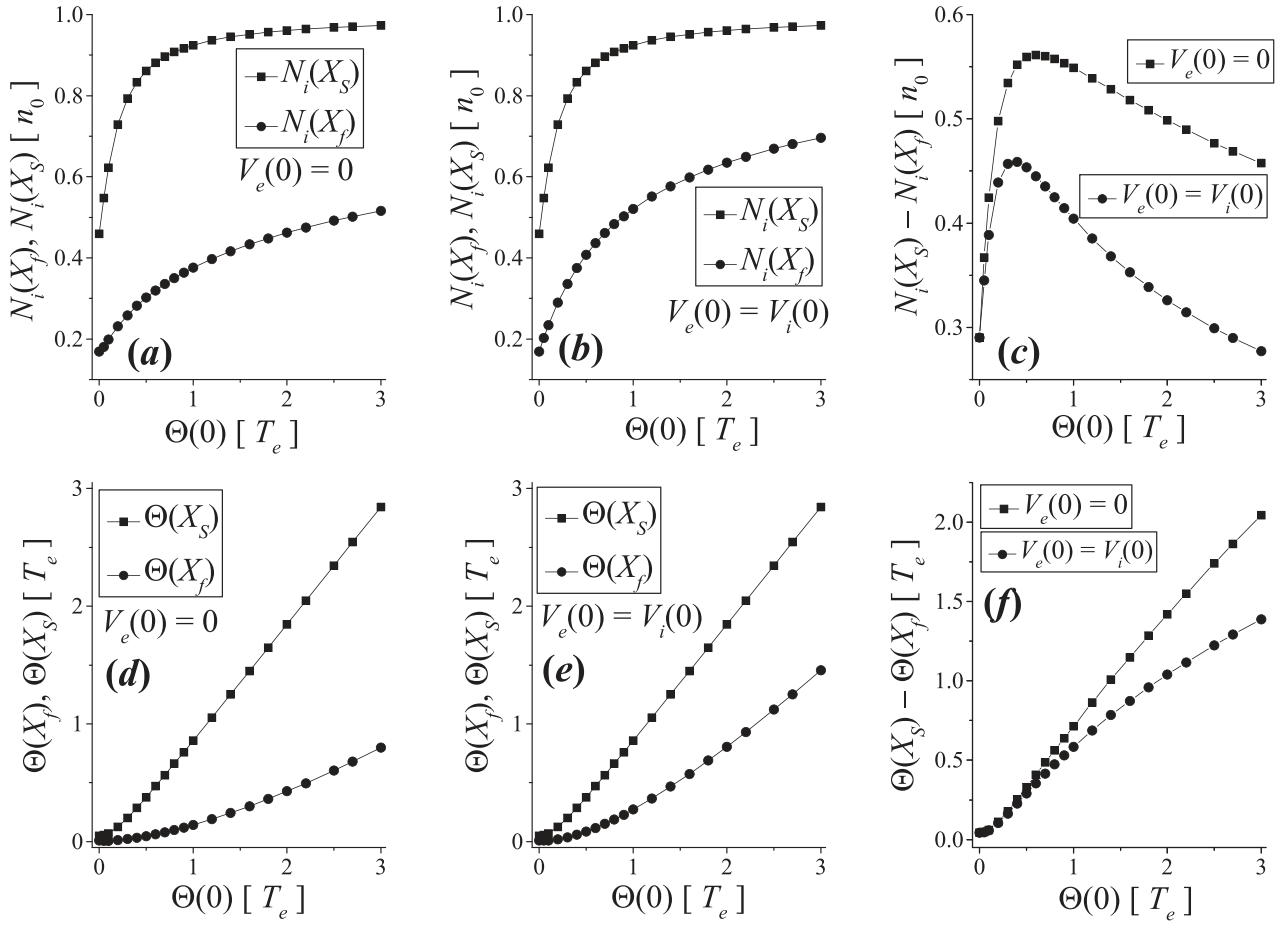

FIG. 13. In the top graphs (a), (b), and (c) ion density $N_i(X_f)$ at the singularity point, ion density at the sheath edge $N_i(X_S)$ and their difference $N_i(X_S) - N_i(X_f)$ are shown versus $\Theta(0)$, for two different boundary conditions $V_e(0) = 0$ and $V_e(0) = V_i(0)$. In the bottom plots (d)–(f), ion temperature $\Theta(X_f)$ at the singularity point, ion temperature at the sheath edge $\Theta(X_S)$ and their difference $\Theta(X_S) - \Theta(X_f)$ are shown versus $\Theta(0)$, for two different boundary conditions $V_e(0) = 0$ and $V_e(0) = V_i(0)$.

edge $V_e(X_S)$ also results in a smaller ion density drop $N_i(X_S) - N_i(X_f)$ in the sheath—see graph (*c*). The same is also valid for the ion temperature drop in the sheath. In plots (*d*) and (*e*), one can see that the ion temperature at the sheath edge is the same for both boundary conditions $V_e(0) = 0$ and $V_e(0) = V_i(0)$. But the ion temperature at the singularity $\Theta(X_f)$ is larger at $V_e(0) = V_i(0)$, and consequently, the temperature drop in the sheath is smaller. The ion temperature drop in the sheath $\Theta(X_f) - \Theta(X_S)$ increases with increasing $\Theta(0)$.

IV. SOME REMARKS ON THE CLOSURE OF THE FLUID EQUATIONS—EFFECTS OF THE ION HEAT FLUX

As it is very well known (see, e.g., Ref. 36), the fluid equations are derived from the moments of the Boltzmann equation. When the Boltzmann equation is multiplied by the mass of the particle and integrated over velocity, the transport equation (or the continuity equation) for the respective particle species is obtained. The continuity equation contains two unknown functions of space—the particle density and the flux, which are the zeroth and the first moment of the velocity distribution function. When the Boltzmann equation is multiplied by the particle momentum and integrated over velocity, the momentum transport equation (or equation of motion) is obtained. This equation contains an additional unknown function—the pressure gradient. The pressure is the second moment of the velocity distribution function. When the Boltzmann equation is multiplied by the kinetic energy of the particle and integrated over velocity, the energy transport equation is obtained. In this equation, an additional unknown function appears—namely, the divergence of the heat flux vector. The heat flux vector is the third moment of the velocity distribution function. The ion heat flux vector in one dimension is given by

$$q_i = \frac{1}{2} m_i \int (v - u_i)^3 f_i(v) dv = \frac{1}{2} m_i n_i \langle w_i^3 \rangle,$$

where

$$w_i \equiv v - u_i, \quad u_i = \frac{\int v f_i(v) dv}{\int f_i(v) dv} = \frac{\int v f_i(v) dv}{n_i}.$$

The ion thermal velocity w_i has been defined. When successive moments of the Boltzmann equation are taken, one is always left with one unknown function more than there are equations in the system to be solved. So, the closure has to

be made by some assumption about the highest moment of the velocity distribution function or by using some information about this function which comes from outside of this analysis. In this work, the closure for the electrons has been made by the assumption that the electrons are isothermal, and so, the electron pressure gradient is proportional to the electron density gradient. The proportionality factor is a constant electron temperature T_e, which is used for normalization of the ion temperature and of the potential—see Eq. (17). For the ions, the closure has been made by the assumption that the ion heat flux is zero, $q_i = 0$. Such closure is very common and it is called the adiabatic approximation of the warm plasma model. Such approximation is justified when the plasma conditions are such that the ion velocity distribution function remains symmetric (Maxwellian or drifted Maxwellian) in the entire plasma system,[37] and consequently, $\langle w_i^3 \rangle = 0$. Of course, there are many mechanisms, which can make the ion distribution function asymmetric in such a way that $\langle w_i^3 \rangle \neq 0$.[37] The analysis of such mechanisms is far beyond the scope of this work. If deviation of ion distribution function from symmetric shape is small enough, the ion heat flux is proportional to the temperature gradient.[37] In one dimension, q_i is then written in the form

$$q_i = -K' \frac{dT_i}{dx}, \tag{26}$$

where K' is the heat conduction coefficient. The steady-state one-dimensional energy transport equation for the ions reads

$$\frac{1}{2} u_i \frac{dp_i}{dx} + \frac{3}{2} p_i \frac{du_i}{dx} + \frac{dq_i}{dx} = m_i f_{CX} n_i u_i^2 + \frac{1}{2} m_i u_i^2 \frac{n_e}{\tau}. \tag{27}$$

Equations (18) and (20) have been taken into account. When (26) is inserted into (27), one gets

$$\frac{1}{2} u_i \frac{dp_i}{dx} + \frac{3}{2} p_i \frac{du_i}{dx} - K' \frac{d^2 T_i}{dx^2} = m_i f_{CX} n_i u_i^2 + \frac{1}{2} m_i u_i^2 \frac{n_e}{\tau}. \tag{28}$$

The heat conduction coefficient K' can be modeled using the kinetic theory of gases. It turns out that it is strongly temperature dependent,[37] and since temperature is space dependent, K' is also space dependent. But in order to illustrate the effect of the heat flux, we will treat it as a given constant coefficient. Using Eq. (17), Eq. (28) is written in one of the following forms:

$$\frac{1}{2} V_i \frac{dP_i}{d\xi} + \frac{3}{2} P_i \frac{dV_i}{d\xi} - K_1 \frac{d^2 \Theta}{d\xi^2} = Z_{CX} N_i V_i^2 + \frac{1}{2} N_e V_i^2, \tag{29}$$

or

$$\frac{1}{2} V_i \frac{dP_i}{dX} + \frac{3}{2} P_i \frac{dV_i}{dX} - K_2 \frac{d^2 \Theta}{dX^2} = \varepsilon Z_{CX} N_i V_i^2 + \varepsilon \frac{1}{2} N_e V_i^2, \tag{30}$$

where

$$K_1 = K' \frac{\tau}{k n_0 L^2}, \quad K_2 = K' \frac{\tau}{k n_0 L \lambda_D} \tag{31}$$

are dimensionless heat conduction coefficients.

In Fig. 14, an example of the solution of the system of Eqs. (9)–(13), (15), (16), and (30) is shown. The same parameters as in Fig. 10 are selected, so that some comparison is possible: $\mu = 1/3670.482$, $\varepsilon = 2 \times 10^{-4}$, and $Z_{CX} = 1$. The boundary conditions are $\Psi(0) = 0$, $N_i(0) = N_e(0) = 1$, $V_e(0) = 0$, and $P_i(0) = \Theta(0) = 0.3$. The ion velocity and electric field are found by the method presented in Fig. 3 and they are $V_i(0) = 0.948683$ and $\chi(0) = 0.001423$. Since Eq. (30) has a term with the second derivative of ion temperature, the first derivative must be specified as a boundary condition. The value $\frac{d\Theta}{dX}(0) = 0$ is selected. In this way, neither ion heating nor cooling is enforced at the boundary. Before systems (9)–(16) with (14) replaced by Eq. (30) can be solved, the ion heat conduction coefficient must be selected. The selection of this value is rather arbitrary, and it is one of the weak points of the presented model. Based on discussion in Sec. IX.6 in Ref. 37, the value $K' = 1$ W/mK is selected. In order to obtain K_2 from Eq. (31), specific plasma parameters must be selected. The inclusion of ion heat flux into the model through replacing Eq. (14) by (30) or (6) by (29), therefore, reduces the generality of the model. Plasma density and electron temperature that could correspond to the edge plasmas in medium or small tokamaks, e.g., COMPASS,[38] are selected: $kT_e = 5$ eV and $n_0 = 10^{18}$ m^{-3}. This gives the Debye length $\lambda_D = 1.662 \times 10^{-5}$ m. The mass of a deuterium ion is $m_i = 3.34 \times 10^{-27}$ kg. The normalizing velocity is then $c_0 = 15486$ m/s, and together with $\varepsilon = 2 \times 10^{-4}$, the ionization length $L = 0.0831$ m is calculated. From c_0 and L, the ionization time $\tau = 5.37 \times 10^{-6}$ s is obtained. Using all these results and formula (31), finally $K_2 = 281548$ is found and inserted into Eq. (30).

Profiles of the potential $\Psi(X)$, electric field $\chi(X)$, ion and electron density $N_{ie}(X)$, and ion and electron velocity $V_{ie}(X)$ are very similar as shown in figures in Sec. III. Intersection of the ion velocity $V_i(X)$ and ion sound velocity $V_S(X)$ in plot (*d*) reveals the location X_S of the sheath edge. The sheath edge X_S is marked by a thin vertical line also in all other plots. But the ion temperature profiles $\Theta(X)$ shown in graph (*f*) is very different than the ion temperature profiles presented in Figs. 1, 2, and 7–10. The ion temperature shown in Fig. 14(f) is almost constant in the entire solution domain. This is understandable, since very large heat conduction coefficient allows heat fluxes, which immediately "smooth out" any temperature gradients that could appear for any reason. What is much less understandable is that ion temperature also increases in the sheath region. In Section II, mechanisms of ion heating in the pre-sheath have been identified. The first is the transfer of electric field energy into ion thermal energy (see Fig. 9), and the second are charge exchange collisions (see Fig. 10). But in both cases, ions are then strongly cooled in the sheath. This cooling is due to adiabatic expansion of ions and this expansion is caused by their strong acceleration by the electric field present in the sheath. Electric field in Fig. 14(b) is even larger than electric fields in Figs. 9 and 10, so even stronger ion acceleration and adiabatic cooling could be expected. The result which implies that the ions are heated also in the sheath is a consequence of our approximation that the heat conduction coefficient is constant everywhere in the system, including the sheath. In a

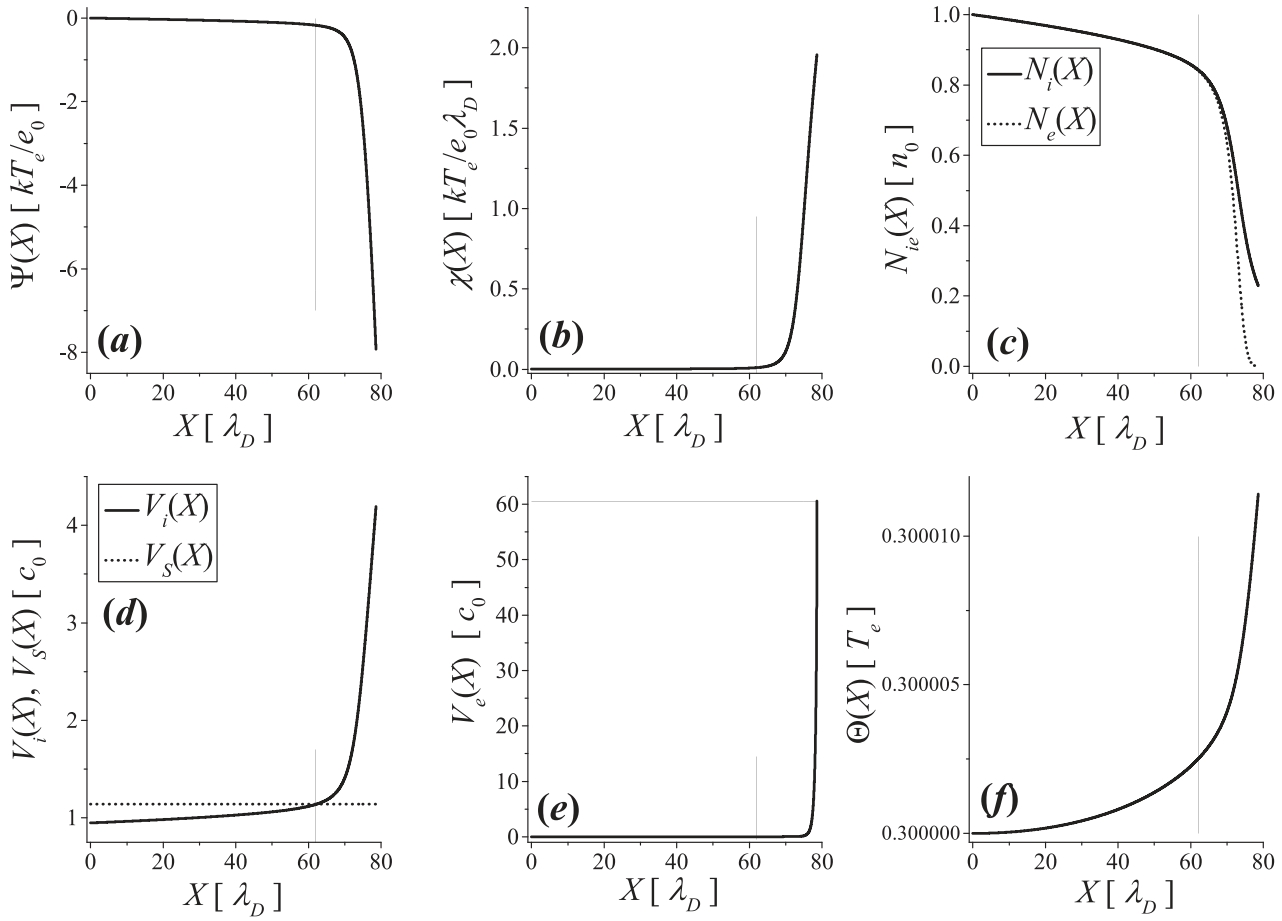

FIG. 14. An example of the solutions of systems (9)–(13), (15), (16), and (30) for the following parameters and boundary conditions: $\mu = 1/3670.482$, $\varepsilon = 2 \times 10^{-4}$, $Z_{CX} = 1$, $K_2 = 281548$, $\Psi(0) = 0$, $N_i(0) = N_e(0) = 1$, $V_e(0) = 0$, $P_i(0) = \Theta(0) = 0.3$, $V_i(0) = 0.948683$, $\chi(0) = 0.001423$ and $\frac{d\Theta}{dX}(0) = 0$.

more realistic model, one should take into account that the heat conduction coefficient is space dependent and it becomes negligibly small in the sheath. The problem of conductive versus convective sheath energy transmission has been studied by Tang and Guo.[39] Their conclusion based on particle in cell simulations is that the main energy transmission mechanism for the ions is convection, while in the case of electrons also conduction plays an important role.

In Figs. 15 and 16, individual terms of Eqs. (14) and (30) are analyzed separately. For practical purposes, the following notation is introduced:

$$A_1(X) = \frac{1}{2} V_i \frac{dP_i}{dX}, \quad A_2(X) = \frac{3}{2} P_i \frac{dV_i}{dX}, \quad A_3(X) = -K_2 \frac{d^2\Theta}{dX^2},$$
$$A_4(X) = \varepsilon Z_{CX} N_i V_i^2, \quad A_5(X) = \varepsilon \frac{1}{2} N_e V_i^2,$$
$$B_j(X) = \int A_j(X) dX, \quad j = 1,2,3,4,5. \tag{32}$$

Once the profiles of $N_i(X)$, $N_e(X)$, $V_i(X)$, and $\Theta(X)$ are found from the system (9)–(16) or (9)–(13), (15), (16), and (30), the profiles of $A_1(X)$ to $A_5(X)$ can be obtained easily. The profiles $B_1(X)$ to $B_5(X)$ are obtained by numerical integration of the respective profiles $A_j(X)$.

In Fig. 15, the profiles of $A_1(X)$, $A_2(X)$, $A_4(X)$, and $A_5(X)$ found from the solutions of systems (9)–(16) are presented in plots (*a*) and (*b*), while the respective $B_1(X)$, $B_2(X)$, $B_4(X)$, and $B_5(X)$ are displayed in graphs (*d*) and (*e*). In plot (*c*), the negative second derivative of the ion temperature $-\frac{d^2\Theta}{dX^2}$ is shown, and in (f), the negative derivative of the ion temperature $-\frac{d\Theta}{dX}$ is presented. The solution of systems (9)–(16), which is shown in Fig. 10, is selected. The parameters and boundary conditions are $\mu = 1/3670.482$, $\varepsilon = 2 \times 10^{-4}$, $Z_{CX} = 1$, $\Psi(0) = 0, N_i(0) = N_e(0) = 1, V_e(0) = 0, P_i(0) = \Theta(0) = 0.3, V_i(0) = 0.948683$, and $\chi(0) = 9.48683 \times 10^{-4}$.

Term $A_1(X)$ gives the spatial profile of the rate of change of internal energy density of ion fluid. The term $A_2(X)$ describes the energy density loss or gain due to expansion or compression of ion fluid. The terms $A_4(X)$ and $A_5(X)$ give the energy density loss or gain due to charge exchange and ionization collisions. In plot (*a*), the profiles of $A_1(X)$ and $A_2(X)$ found from the solutions of systems (9)–(16) are displayed. As the ion fluid flows towards the wall in the positive X direction, it is expanded, and consequently, the work is done by the fluid. So, the profile $A_2(X)$ is positive everywhere in the system. Because the work has been done during ion expansion, the ion fluid loses its internal energy, and this results in a negative profile $A_1(X)$. But the loss of internal energy is not exactly equal to the work done, because energy loss by the work done is partially (but only in a very small fraction) compensated by charge exchange and ionization collisions. This can be seen in positive profiles $A_4(X)$ and $A_5(X)$ displayed in plot (*b*). These two terms are on the right hand side of Eq. (14), and therefore, they must be subtracted

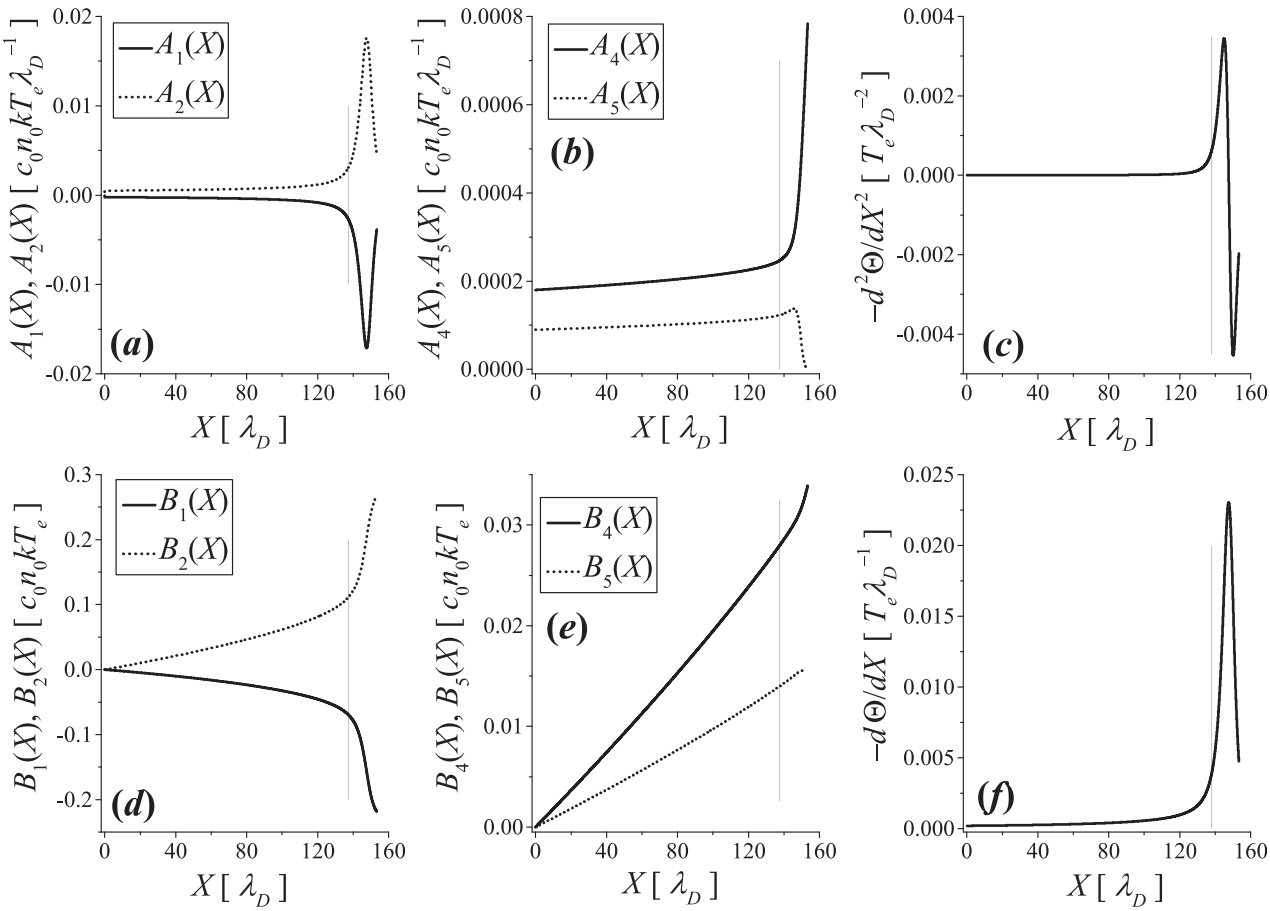

FIG. 15. Profiles of $A_j(X)$ and $B_j(X)$ found from the solutions of the system (9)–(16) together with the negative first and second derivative of the ion temperature. Selected parameters and boundary conditions are $\mu = 1/3670.482$, $\varepsilon = 2 \times 10^{-4}$, $Z_{CX} = 1$, $\Psi(0) = 0$, $N_i(0) = N_e(0) = 1$, $V_e(0) = 0$, $P_i(0) = \Theta(0) = 0.3$, $V_i(0) = 0.948683$, and $\chi(0) = 9.48683 \times 10^{-4}$. Thin vertical line indicates the position of the sheath edge.

from $A_2(X)$. In any case, their contribution is almost negligible, since they are more than 2 orders of magnitude smaller than $A_1(X)$ and $A_2(X)$. In accordance with Eq. (14), the sum $A_1(X) + A_2(X) - A_4(X) - A_5(X)$ is zero.

In the pre-sheath region, both $A_1(X)$ and $A_2(X)$ are very close to zero, but in the sheath they both change strongly. The position of the sheath edge is indicated by a thin vertical line and it is determined as shown in Fig. 2. The minimum value of A_1 is -0.01708, and the maximum value of A_2 is 0.01757. The maximum value of A_4 is 7.833×10^{-4}, and the maximum value of A_5 is 1.372×10^{-4}. The terms A_1 to A_5 have the units of $c_0 n_0 kT_e \lambda_D^{-1}$. If the same plasma parameters as above are selected ($n_0 = 10^{18}$ m^{-3}, $kT_e = 5$ eV, $\lambda_D = 1.662 \times 10^{-5}$ m, and $c_0 = 15486$ m/s), one unit of $c_0 n_0 kT_e \lambda_D^{-1}$ corresponds to power density 7.46363×10^8 W/m^3. So, the minimum value of A_1 corresponds to -1.27479×10^7 W/m^3, while the maximum values of A_2, A_4, and A_5 correspond to 1.31136×10^7, 584626, and 102401 W/m^3, respectively.

The profiles $B_j(X)$ give the corresponding energy fluxes in the units of $c_0 n_0 kT_e$. For the "standard plasma parameters" $n_0 = 10^{18}$ m^{-3}, $kT_e = 5$ eV, and $c_0 = 15486$ m/s one unit of $c_0 n_0\ kT_e$ corresponds to 12404 W/m^2. The profile $B_1(X)$ [plot (*d*)] is negative and decreases monotonically with a sharp jump in the sheath. This indicates energy flow in the direction from the wall towards the bulk plasma, because the ion fluid loses its internal energy as it flows towards the wall. On the other hand, $B_2(X)$ is positive and increases monotonically and also has a sharp jump in the sheath. Energy flow that corresponds to expansion of ion fluid has positive direction from the plasma towards the wall. Energy fluxes $B_4(X)$ and $B_5(X)$, which are due to collisions, are in agreement with (32) and plotted as positive in graph (*e*), but in fact, the corresponding energy flow is directed from the wall to the plasma, because the ion fluid gains more and more energy from collisions as it flows towards the wall. The flux balance is given by $B_1(X) + B_2(X) - B_4(X) - B_5(X)$. Note that $B_1(X)$ is negative, while $B_2(X), B_4(X)$, and $B_5(X)$ are positive, and the total energy flux in the ion fluid is zero. At the singularity point of the system $X = X_f$, the values of the energy fluxes given in the units $c_0 n_0 kT_e$ are the following: $B_1(X_f) = -0.21823$, $B_2(X_f) = 0.26772$, $B_3(X_f) = 0.033915$, and $B_4(X_f) = 0.01558$. It can be noticed that $B_1(X_f) + B_2(X_f) - B_4(X_f) - B_5(X_f)$ is indeed zero within the limits of numerical precision. The corresponding values in units W/m^2 for the plasma parameters given earlier are as follows: $B_1(X_f) = -2707.01$, $B_2(X_f) = 3320.91$, $B_3(X_f) = 420.695$, and $B_4(X_f) = 193.261$.

Finally, both derivatives of ion temperature [$-\frac{d^2\Theta}{dX^2}$ - plot (*c*) and $-\frac{d\Theta}{dX}$—graph (*f*)] need some explanation. In the pre-sheath region, both derivatives are very close to zero, because in this region, the ion temperature changes very little. Only in the sheath, both derivatives exhibit strong jumps,

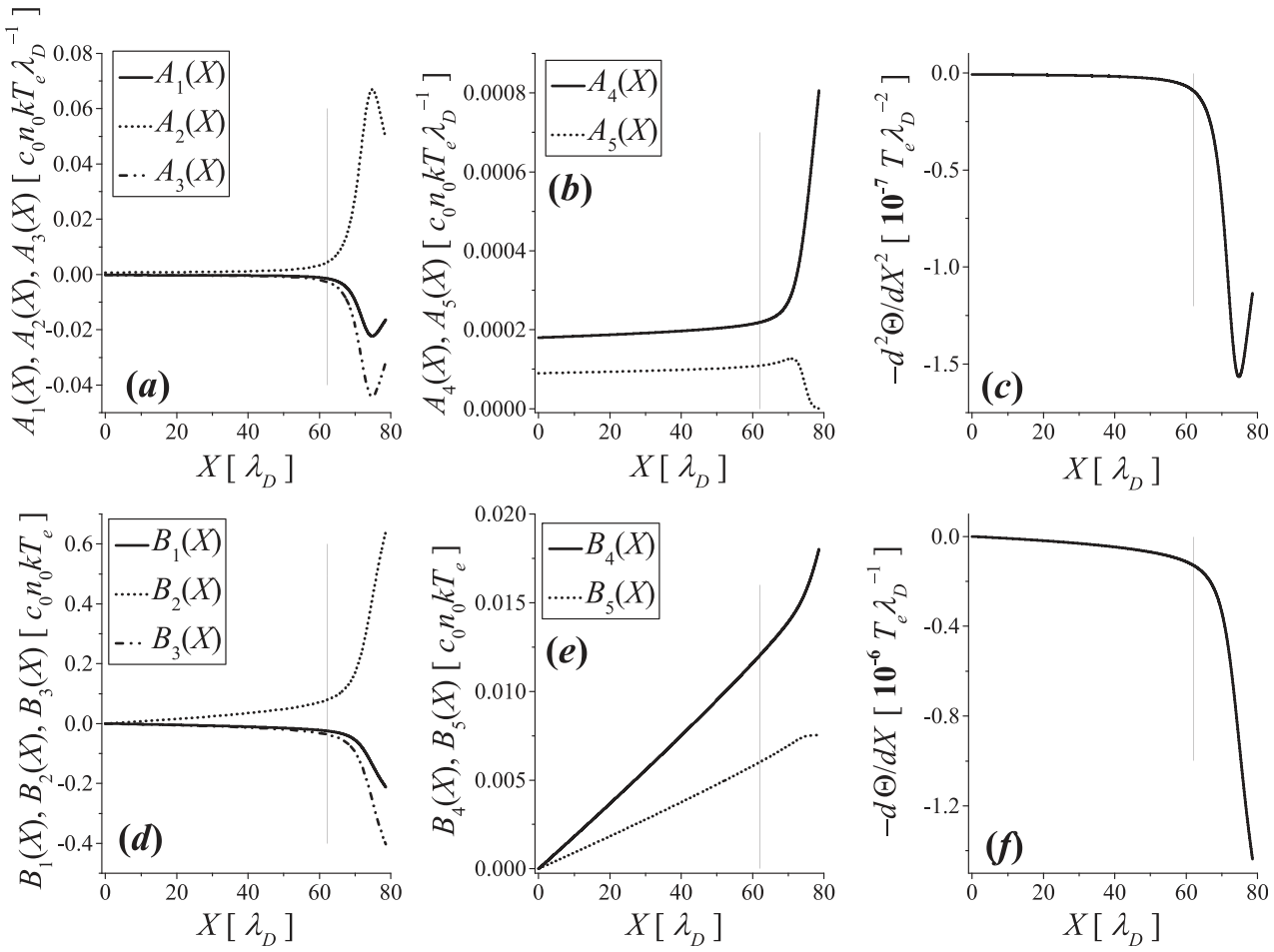

FIG. 16. Profiles of $A_j(X)$ and $B_j(X)$ found from the solutions of the system (9)–(13), (15), (16), and (30) together with the negative first and second derivative of the ion temperature. The selected parameters and boundary conditions are $\mu = 1/3670.482$, $\varepsilon = 10^{-4}$, $Z_{CX} = 0.2$, $\Psi(0) = 0$, $N_i(0) = N_e(0) = 1$, $V_e(0) = 0$, $P_i(0) = \Theta(0) = 0.4$, $V_i(0) = 1.095445$, $\chi(0) = 0.001205$, $\frac{d\Theta}{dX}(0) = 0$ and $K = 2.81548 \times 10^9$. Thin vertical line indicates the position of the sheath edge.

because ion temperature drops strongly in the sheath. According to Eq. (30), the second derivative $-\frac{d^2\Theta}{dX^2}$ is proportional to term $A_j(X)$, which gives the rate of change of energy of the ion fluid due to various reasons. The maximum value of $-\frac{d^2\Theta}{dX^2}$ in Fig. 15(c) is 0.00344 given in the units $T_e\lambda_D^{-2}$. For electron temperature $kT_e = 5$ eV and plasma density $n_0 = 10^{18}$ m^{-3}, the Debye length is $\lambda_D = 1.662 \times 10^{-5}$, and electron temperature is $T_e = 58043$ K. So, the peak value of $-\frac{d^2\Theta}{dX^2}$ corresponds to 7.22872×10^{11} K/m^2. In order to estimate the corresponding power density, some heat conduction coefficient should be selected. When the system (9)–(13), (15), (16), and (30) has been solved (Fig. 14), $K' = 1$ W/mK has been selected, and then, $K_2 = 281548$ has been found using the formula (31) and the values $n_0 = 10^{18}$ m^{-3}, $\lambda_D = 1.662 \times 10^{-5}$, $L = 0.0831$ m, $k = 1.38 \times 10^{-23}$ J/K, and $\tau = 5.36602 \times 10^{-6}$ s. Then, $K_2 = 281548$ has been inserted into Eq. (30). This time the procedure is reversed. From the maximum value of $-\frac{d^2\Theta}{dX^2}$, which is 0.00344 and the maximum value of A_2, which is 0.01757, one estimates $K_2 \sim 5.11$. Using the same values as above, $n_0 = 10^{18}$ m^{-3}, $\lambda_D = 1.662 \times 10^{-5}$, $L = 0.0831$ m, $k = 1.38 \times 10^{-23}$ J/K, and $\tau = 5.36602 \times 10^{-6}$ s, formula (31) gives $K' = 1.81 \times 10^{-5}$ W/mK. Such negligibly small heat conduction is consistent with convective (and not conductive) energy transfer through the sheath (see also Ref. 39).

Similar estimation can be done also from the first derivative $-\frac{d\Theta}{dX}$. The peak value of the first derivative shown in plot (*f*) is 0.02303. It is given in the units of $T_e\lambda_D^{-1}$. For the earlier given plasma density, electron temperature, and Debye length, this corresponds to 8.043×10^7 K/m. The first derivative of the ion temperature $-\frac{d\Theta}{dX}$ is proportional to the energy fluxes given by terms B_j. The maximum value of $B_2(X)$ is $B_2(X_f) = 0.26772$. In a similar way as above, one estimates that $K_2 \sim 11.62$. Using $n_0 = 10^{18}$ m^{-3}, $\lambda_D = 1.662 \times 10^{-5}$, $L = 0.0831$ m, $k = 1.38 \times 10^{-23}$ J/K, $\tau = 5.36602 \times 10^{-6}$ s, and formula (31), we get $K' = 4.13 \times 10^{-5}$ W/mK, which is the same order of magnitude as above.

In Fig. 16, the profiles of $A_1(X)$, $A_2(X)$, $A_3(X)$, $A_4(X)$, and $A_5(X)$ found from the solutions of systems (9)–(13), (15), (16), and (30) are presented in plots (a) and (b), while the respective $B_1(X)$, $B_2(X)$, $B_3(X)$, $B_4(X)$, and $B_5(X)$ are displayed in graphs (d) and (e). In plot (c), the negative second derivative of the ion temperature $-\frac{d^2\Theta}{dX^2}$ is shown, and in (f), the negative derivative of the ion temperature $-\frac{d\Theta}{dX}$ is presented. The respective solution of systems (9)–(13), (15), (16), and (30) is shown in Fig. 14, and the parameters and boundary

conditions are as follows: $\mu = 1/3670.482$, $\varepsilon = 10^{-4}$, $Z_{CX} = 1$, $\Psi(0) = 0$, $N_i(0) = N_e(0) = 1$, $V_e(0) = 0$, $P_i(0) = \Theta(0) = 0.3$, $V_i(0) = 0.948683$, $\chi(0) = 0.001423$, $\frac{d\Theta}{dX}(0) = 0$ and $K_2 = 281548$. In plot (*a*), the profiles of $A_1(X)$, $A_2(X)$, and $A_3(X)$ found from the solutions of systems (9)–(13), (15), (16), and (30) are displayed. The profile $A_1(X)$ is negative, because the ions are losing internal energy, as they flow towards the wall. The profile $A_2(X)$ is positive, because the work is done by the ion fluid during its expansion as it flows towards the wall. The profile $A_3(X)$ is negative. This is a consequence of the result shown in Fig. 14(f), which indicates that the ions are heating, as they flow towards the wall and so the second derivative $-\frac{d^2\Theta}{dX^2}$ is negative. The reasons for such surprising result have been discussed in relation to Fig. 14. The energy balance given by Eq. (30) can be qualitatively described in the following way. As the ion fluid flows towards the wall, it is expanded, and consequently, work is done, and this results in positive profile of $A_2(X)$. Because the work is done by the ion fluid, its internal energy decreases, resulting in a negative profile $A_1(X)$. But the decrease in internal energy is smaller than the work done, because it is partially compensated by charge exchange and ionization collisions [positive profiles of $A_4(X)$ and $A_5(X)$ shown in plot (*b*), which are on the right hand side of Eq. (30)] and especially by the heat flow in the direction from the wall towards the bulk plasma, i.e., in the direction of the negative X axis. This results in negative profile $A_3(X)$. The sum $A_1(X) + A_2(X) + A_3(X) - A_4(X) - A_5(X)$ is zero, and total energy is conserved.

Similarly, as in Fig. 15, the profiles in the pre-sheath region the profiles $A_1(X)$, $A_2(X)$, and $A_3(X)$ are very close to zero, but in the sheath, a very strong jump of the respective curves can be observed. The maximum value of A_2 is 0.06692, while the minimum values of A_1 and A_3 are -0.0223 and -0.04408, respectively. Note that extreme values of A_1 and A_2 are larger than the respective values in Fig. 15. The maximum values of A_4 and A_5 shown in plot (*b*) are 8.063×10^{-4} and 1.2712×10^{-4}, respectively. These values on the other hand are much closer to the corresponding values in Fig. 15.

Additional heat conduction term in Eq. (30) with a heat conduction coefficient K_2 assumed to be constant everywhere introduces an additional ion heating mechanism into the system. This results in constant ion heating in the direction of positive X. If, in addition, the heat conduction coefficient is large, there is a constant heat flow in the negative direction of X, and so, the increase in ion temperature is very small. In plot (*d*), indeed a rather large negative heat flux $B_3(X)$ is clearly visible. The largest value, given in the units of $c_0 n_0 k T_e$, is at the wall, $B_3(X_f) = -0.40442$. For plasma density $n_0 = 10^{18}$ m^{-3} and electron temperature $kT_e = 5$ eV, this corresponds to -5016.59 W/m^2.

Both derivatives of ion temperature, displayed in graphs (*c*) and (*e*), are four orders of magnitude smaller than the corresponding derivatives shown in Fig. 15. The maximum value of $-\frac{d^2\Theta}{dX^2}$ in Fig. 15(c) is 0.00344, while the minimum value of $-\frac{d^2\Theta}{dX^2}$ in Fig. 16(c) is -1.566×10^{-7}. The maximum value of $-\frac{d\Theta}{dX}$ in Fig. 15(f) is 0.02303, while the minimum value of $-\frac{d\Theta}{dX}$ in Fig. 16(f) is -1.44×10^{-6}.

V. CONCLUSIONS

A one-dimensional, steady state, self-consistent, two-fluid model has been used to analyze the effects of ion temperature to the plasma wall transition in front of a negative planar electrode. Continuity and momentum exchange equations are used for the electrons, while the continuity, momentum exchange, and energy exchange equations are used for singly charged positive ions. The electrons are assumed to be isothermal, while for the ions, the closure is made by the assumption that the heat flux is zero. Equations of the model are solved numerically with a finite value of ε. The ion temperature is treated as a given, independent parameter, which is included in the model as a boundary condition. Because the system of equations becomes singular if the ion velocity V_i drops below the ion thermal velocity V_{ith}, finite $\Theta(0)$ means that also $V_i(0)$ must be above a certain minimum value. A numerical procedure how to find this minimum value of $V_i(0)$ together with the corresponding electric field $\chi(0)$ or $\eta(0)$ is proposed. If ion temperature $\Theta(0)$ is increased, the minimum ion velocity $V_i(0)$ and the corresponding electric field $\chi(0)$ also increase. In the limit of very large ion temperatures $V_i(0)$ approaches to the ion sound velocity V_S and the boundary $X = 0$ approaches to the sheath edge X_S. It has been shown that the minimum velocity $V_i(0)$, which is found together with the corresponding electric field $\chi(0)$ or $\eta(0)$, corresponds to the ion thermal velocity $\sqrt{\kappa(0)\Theta(0)}$ with $\kappa(0) = 3$. At $\xi = 0$ or $X = 0$ the ion flow is adiabatic. In the pre-sheath region, the ions are accelerated in the positive direction of ξ or X, and at the same time, they also receive thermal energy. The presented model can describe two sources of ion thermal energy. The first is the electric field, and the second are charge exchange collisions. If $\Theta(0)$ and also consequently $V_i(0)$ are low enough, so that ion expansion is slow enough, the ions receive more energy from these two sources than is the work done during their expansion. In this case, ions are heating and expanding at the same time. Close to the sheath edge and in the sheath, the ion acceleration always [irrespective of $\Theta(0)$] becomes so strong that their thermal energy is converted into kinetic energy of ion beam and so in this region the ions are always cooled down. If, on the other hand, $\Theta(0)$ and $V_i(0)$ are large enough, the ion expansion is so fast that the ion temperature is a monotonically decreasing function of ξ or X, but in a large part of the pre-sheath their thermal energy loss due to expansion is partially compensated from both sources mentioned above. So, in this region, the cooling of ions is slower than it should be due to the work done by their expansion.

In the model presented in this work, the ions are, therefore, neither isothermal[9–17] nor adiabatic.[18–22] Instead, it is possible to find the spatial profile of the ion temperature $\Theta(X)$ and of the polytropic function $\kappa(X)$ as solutions of the model equations. Ion flow is adiabatic only at the boundary $X = 0$ of the system and close to the sheath edge and inside the sheath. Nevertheless, basic conclusions on ion temperature effects are basically the same as in isothermal[17] and/or adiabatic[21] models, where the polytropic coefficient is treated as a given constant. These conclusions are larger ion temperature results in larger excess of positive space charge

in the sheath, and on average, larger electric field in the sheath region. But there is one important difference between two fluid models presented here and models where the fluid equations for the electrons are replaced by the Boltzmann relation. In the two-fluid model, the potential drop in the sheath depends on the selection of the boundary condition $V_e(0)$ for the electron velocity. If $V_e(0) = 0$ is selected, electron velocity at the sheath edge $V_e(X_S)$ decreases with the increase in ion temperature $\Theta(0)$. Because of that the "sheath potential drop" also increases. The "sheath thickness," that is, the distance $X_f - X_S$ between the sheath edge X_S and the singularity X_f of model equations, decreases with increasing ion temperature. In this case indeed, as expressed by Ref. 21, larger ion temperature produces better shielding of biased electrode from the plasma. If on the other hand the boundary condition $V_e(0) = V_i(0)$ is selected, the electron velocity at the sheath edge $V_e(X_S)$ increases with increasing ion temperature $\Theta(0)$ and it is approximately equal to the ion sound velocity at the sheath edge. Because of increasing $V_e(X_S)$ the" sheath potential drop" decreases. The "sheath thickness" decreases also and it decreases in such a way, that the average electric field in the sheath still increases with increasing $\Theta(0)$. Also, the positive space charge density in the sheath increases with increasing $\Theta(0)$. So, the conclusion that larger ion temperature produces better shielding of biased electrode from the plasma remains valid also in the case when the boundary condition $V_e(0) = V_i(0)$ is selected.

An attempt has been made to include the ion heat flux vector q_i in the model. The simplest possible relationship between the heat flux q_i and ion temperature T_i has been assumed, namely, $q_i = -K' \frac{dT_i}{dx}$, where K' is a constant heat conduction coefficient. In order to solve the model, some specific value of K' must be assumed. In this work, $K' = 1$ W/mK has been assumed. It is believed that such choice is the correct order of magnitude for the edge plasmas of medium and small tokamaks.[37] By introducing the heat flux in this form on one hand, the generality of the model is reduced since some specific plasma density and electron temperature must be selected, otherwise the heat conduction coefficient in the energy transfer equation cannot be normalized. Such normalization is then valid only for the specifically selected plasma parameters. On the other hand, additional heat conduction term in Eq. (30) with a heat coefficient K_2 assumed to be constant everywhere, introduces a new ion heating mechanism into the system. This results in constant ion heating in the direction of positive X. Such heating of ions takes place even in the sheath. Because the heat conduction coefficient is nonzero, there is a constant heat flow in the negative direction of X. Final result is an almost isothermal ion flow in the entire system including the sheath. Such result of the model does not correspond to widely accepted belief[18–23] that ion flow in the sheath is much closer to adiabatic than to isothermal. Much better, but also mathematically much more complicated way to include the ion heat flux into a fluid model like presented in this work is to make the closure of the fluid equations at a higher moment of the Boltzmann equation. In this way, the system of fluid equations obtains one additional equation, and consequently, a solution for one additional unknown function—the ion heat flux—can be obtained.

ACKNOWLEDGMENTS

This work has been partially supported by the Grant No. P2–0073 of the Slovenian research agency.

[1]K.-U. Riemann, J. Phys. D: Appl. Phys. **24**, 493 (1991).
[2]K.-U. Riemann, J. Tech. Phys. **41**(Special Issue), 89 (2000).
[3]D. Bohm, in *The Characteristics of Electrical Discharges in Magnetic Fields*, edited by A. Guthrie and R. K. Wakerling (McGraw-Hill, New York, 1949), Chap. 3, pp. 77–86.
[4]K.-U. Riemann, Phys. Plasmas **4**, 4158–4166 (1997).
[5]K.-U. Riemann, J. Seebacher, D. D. Tskhakaya, Sr., and S. Kuhn, Plasma Phys. Controlled Fusion **47**, 1949–1970 (2005).
[6]L. Tonks and I. Langmuir, Phys. Rev. **34**, 876–922 (1929).
[7]D. D. Tskhakaya, Sr., L. Kos, and N. Jelić, Phys. Plasmas **21**, 073503 (2014).
[8]L. Kos, D. D. Tskhakaya, Sr., and N. Jelić, Phys. Plasmas **18**, 053507 (2011).
[9]H. Ghomi and M. Khoramabadi, J. Plasma Phys. **76**, 247–255 (2010).
[10]M. Khoramabadi, H. R. Ghomi, and M. Ghorannevis, J. Plasma Fusion Res. SERIES **8**, 1399–1402 (2009).
[11]M. Khoramabadi, H. Ghomi, and M. Ghorannevis, J. Fusion Energy **29**, 365–370 (2010).
[12]M. El Kaouini, H. Chatei, I. Driouch, and M. El Hammouti, J. Fusion Energy **30**, 199–204 (2011).
[13]J. Liu, F. Wang, and J. Sun, Phys. Plasmas **18**, 013506 (2011).
[14]M. El Kaouini and H. Chatei, J. Fusion Energy **31**, 317–324 (2012).
[15]M. M. Hatami and B. Shokri, Phys. Plasmas **20**, 033506 (2013).
[16]J. Ou and J. Yang, Phys. Plasmas **19**, 113504 (2012).
[17]M. Khoramabadi, H. Ghomi, and P. K. Shukla, J. Appl. Phys. **109**, 073307 (2011).
[18]J. I. F. Palop, J. Ballesteros, M. A. Hernández, R. Morales Crespo, and S. Borrego del Pino, J. Appl. Phys. **95**, 4585–4592 (2004).
[19]J. I. F. Palop, J. Ballesteros, V. Colomer, and M. A. Hernández, J. Phys. D: Appl. Phys. **29**, 2832–2840 (1996).
[20]J. I. F. Palop, J. Ballesteros, M. A. Hernández, R. Morales Crespo, and S. Borrego del Pino, J. Phys. D: Appl. Phys. **38**, 868–871 (2005).
[21]J. I. F. Palop, J. Ballesteros, R. M. Crespo, and M. A. Hernández, J. Phys. D: Appl. Phys. **41**, 235201 (2008).
[22]M. Khoramabadi and S. F. Masoudi, Astrophys. Space Sci. **341**, 501 (2012).
[23]A. Tshushima and Y. Saitou, J. Phys. Soc. Jpn. **80**, 045001 (2011).
[24]G. C. Das, B. Singha, and J. Chutia, Phys. Plasmas **6**, 3685 (1999).
[25]E. Zawaideh, F. Najmabadi, and R. W. Conn, Phys. Fluids **29**, 463 (1986).
[26]E. Zawaideh, N. S. Kim, and F. Najmabadi, Phys. Fluids **31**, 3280 (1988).
[27]E. Zawaideh, N. S. Kim, and F. Najmabadi, Phys. Fluids B **2**, 647 (1990).
[28]M. Laux, H. Grote, K. Günther, A. Herrmann, D. Hildebrandt, P. Pech, H.-D. Reiner, H. Wolff, and G. Ziegenhagen, J. Nucl. Mater. **162–164**, 200 (1989).
[29]J. P. Gunn, J. Nucl. Mater. **337–339**, 310 (2005).
[30]I. H. Hutchinson, Phys. Fluids **30**, 3777 (1987).
[31]T. Gyergyek and J. Kovačič, Phys. Plasmas **23**, 063510 (2016).
[32]T. Gyergyek and J. Kovačič, Phys. Plasmas **24**, 063506 (2017).
[33]S. Kuhn, K.-U. Riemann, N. Jelić, D. D. Tskhakaya, Sr., D. Tskhakaya, Jr., and M. Stanojević, Phys. Plasmas **13**, 013503 (2006).
[34]N. Jelić, K.-U. Riemann, T. Gyergyek, S. Kuhn, M. Stanojević, and J. Duhovnik, Phys. Plasmas **14**, 103506 (2007).
[35]T. Gyergyek and J. Kovačič, Contrib. Plasma Phys. **54**, 647 (2014).
[36]J. A. Bittencourt, *Fundamentals of Plasma Physics*, 3rd ed. (Springer, New York, 2004).
[37]P. C. Stangeby, *The Plasma Boundary of Magnetic Fusion Devices* (IoP Publishing, Bristol/Philadelphia, 2000).
[38]M. Dimitrova1, R. Dejarnac, T. K. Popov, P. Ivanova, E. Vasileva, J. Kovačič, J. Stocke1, J. Havlicek, F. Janky, and R. Panek, Contrib. Plasma Phys. **54**, 255 (2014).
[39]X.-Z. Tang and Z. Guo, Phys. Plasmas **22**, 100703 (2015).